Delivery report

# Development and validation of a global GPP/NPP model using MERIS and Sentinel-3 data (TerrA-P)

## ATBD v2.2

Iain Colin Prentice, Rebecca Thomas, Keith Bloomfield, Wenjia Cai

Study accomplished under the authority of ESA

January 2019





## DISTRIBUTION LIST

Philippe Goryl, ESA-ESRIN

Iain Colin Prentice, ICL
Keith Bloomfield, ICL
Wenjia Cai, ICL

Else Swinnen, VITO
Roel Van Hoolst, VITO
Bruno Smets, VITO

Ivan Janssens, UA
Sara Vicca, UA
Manuela Balzarolo, UA

## SUMMARY

The aim of the TerrA-P project is to implement and validate a new global monitoring system for primary production by land ecosystems, comprising dekad composites of gross primary production (GPP) and annual composites of above-ground biomass production (ABP) by $C_3$ and $C_4$ plants. Spectral reflectance data from Sentinel-3 are envisaged to be used in this system to drive a recently developed universal, first-principles light use efficiency model (the 'P' model) for GPP.

This document is version 2.2 of the Algorithm Theoretical Basis Document (ATBD) for these GPP and ABP products. It describes the design criteria adopted by TerrA-P for both products based on a user survey, and also on a set of scientific requirements that go significantly beyond the current state of the art. It includes a brief review of the history of light use efficiency (LUE) models, and summarizes the strengths and weaknesses of various existing LUE models including those used operationally. It is shown how the P model – with the linear mathematical form of a LUE model – can be derived from the standard (non-linear) model of photosynthesis via explicit hypotheses for the environmentally induced acclimation of three parameters of the standard model. In comparisons with GPP derived from eddy-covariance carbon dioxide ($CO_2$) flux measurements, the P model has been shown to achieve comparable accuracy to other LUE models, while requiring fewer parameters to be estimated.

Just one parameter, the intrinsic quantum efficiency of $C_3$ photosynthesis $\phi_0(C_3)$, was calibrated to optimize the agreement of modelled and observed GPP across 17 eddy-covariance carbon dioxide ($CO_2$) flux measurement sites. The sites were selected for their relatively homogeneous surrounding vegetation and long measurement records. ATBD version 2.1 introduced an update to the calibration presented in version 1. In the version 2.1 calibration, also shown here, remotely sensed land surface temperature (LST) was used as an alternative to site-measured air temperature to provide temperature and vapour pressure deficit drivers. This calibration used the same merged input data set as in version 1, based on spectral reflectances from SeaWiFS and MERIS, to provide the fraction of incident photosynthetically active radiation absorbed by green tissues (fAPAR). Meteorological data other than temperature were derived from site measurements as before. The new optimized value of $\phi_0(C_3)$ was 0.092, slightly higher than the value presented in version 1 but still within the range expected based on leaf-level measurements. This version (2.2) also includes an extension of the GPP algorithm in which the Copernicus Soil Water Index has been used, together with an independently developed empirical function relating the fractional decrease in GPP to soil moisture, to adjust the GPP generated by the P model for drought conditions.

The model has been applied to data from a larger set of flux measurement sites for validation. Model outputs were supplied based on the new calibration, but driven by new and recently available fAPAR data for these sites. Model outputs for validation, produced along with ATBD version 2.1, included a comprehensive uncertainty propagation scheme which provides time- and location-specific uncertainties for modelled GPP. The validation exercise has been carried out independently by the UA group, and the results presented in a separate Validation Report.

ATBD version 2.1 also outlined the development strategy for the ABP product, and summarized the validation and benchmarking strategies for both products. This version (2.2) presents empirical equations and coefficients to determine the ratio of annual above-ground production to GPP, for application in managed and unmanaged forests, non-forest ecosystems, and croplands. The ABP product consists of the GPP monitoring system together with functions to determine annual ABP from annual GPP, which depend on the ecosystem type and management status, and (in the case of forests) on stand age.

## TABLE OF CONTENTS

## LIST OF FIGURES

## LIST OF TABLES

## LIST OF ACRONYMS

| | |
|---|---|
| 3-PG | Physiological Principles Predicting Growth |
| AATSR | Advanced Along-Track Scanning Radiometer |
| ABP | Above-ground biomass production |
| ABPE | Above-ground biomass production efficiency |
| ATBD | Algorithm Theoretical Basis Document |
| AVHRR | Advanced Very High Resolution Radiometer |
| BESS | Breathing Earth System Simulator |
| BIOME-BGC | Biome–BioGeochemical Cycles model |
| BPLUT | Biome Parameter Look-Up Table |
| CASA | Carnegie-Ames-Stanford Approach model |
| C-Fix | Carbon Fixation model |
| CGLOPS-1 | Copernicus Global Land Operations Lot1 |
| | CHELSA Climatologies at high resolution for the earth's land surface areas |
| CRO | Cropland |
| CUE | Carbon use efficiency |
| DBF | Deciduous broadleaf forest |
| DMP | Dry Matter Productivity algorithm |
| EBF | Evergreen broadleaf forest |
| EC-LUE | Eddy Covariance-Light Use Efficiency model |
| ECMWF | European Centre for Medium-range Weather Forecasts |
| ENF | Evergreen needleleaf forest |
| ET | Evapotranspiration |
| FACE | Free Air Carbon dioxide Enrichment |
| fAPAR, FPAR | Fractional absorbed photosynthetically active radiation |
| | FI Fertilized and/or irrigated |
| FvCB | Farquhar, von Caemmerer and Berry model |
| GLO-PEM | Global Production Efficiency Model |
| GMAO | Global Modeling and Assimilation Office |
| GPP | Gross primary production |
| GVI | Global vegetation index |
| | IGBP International Geopshere-Biosphere Programme |
| IPAR | Incident photosynthetically active radiation |
| LAI | Leaf area index |
| LPJ | Lund-Potsdam-Jena model |
| LPX | Land-surface Processes and eXchanges model |
| LST | Land surface temperature |
| LUE | Light use efficiency |
| | M Otherwise managed |
| | MAT Mean annual temperature |
| MERIS | Medium Resolution Imaging Spectrometer |
| MODIS | Moderate Resolution Imaging Spectroradiometer |
| MTCI | MERIS Total Chlorophyll Index |
| NASA | National Aeronautics and Space Administration |
| NDVI | Normalized difference vegetation index |
| NOAA | National Oceanic and Atmospheric Administration |
| NPP | Net primary production |
| OSH | Open shrubland |
| | Mean annual precipitation |
| P | Production model |

| | |
|---|---|
| PPFD | Photosynthetic photon flux density |
| | RD Recently disturbed |
| RMSE | Root mean squared error of prediction |
| SDBM | Simple Diagnostic Biosphere Model |
| SeaWiFS | Sea-Viewing Wide Field-of-View Sensor |
| | UM Unmanaged or pristine |
| | VEG vegetation type |
| VOC | Volatile organic compound |
| vpd | vapour pressure deficit |

## LIST OF SYMBOLS

| | |
|---|---|
| $C_3$ | photosynthetic pathway whereby carbon is first incorporated into three-carbon sugars |
| $C_4$ | photosynthetic pathway whereby carbon is first incorporated into four-carbon sugars |
| $c_a$ | ambient partial pressure of carbon dioxide [Pa] |
| $c_i$ | leaf-internal partial pressure of carbon dioxide [Pa] |
| C:N | ratio of carbon to nitrogen content [–] |
| $CO_2$ | carbon dioxide |
| $c^*$ | unit cost of maintaining electron transport capacity (P model) [–] |
| $D$ | vapour pressure deficit [kPa] |
| $e_a$ | absolute vapour pressure of water [Pa] |
| $e_s$ | saturation vapour pressure of water [Pa] |
| $f_{BG}$ | fraction of carbon allocated below ground [–] |
| $g_1$ | stomatal sensitivity parameter (Medlyn et al., 2011 model) [$kPa^{0.5}$] |
| | $i_m$ intercept dependent on management |
| $J_{max}$ | maximum rate of electron transport (FvCB model) [µmol $m^{-2}$ $s^{-1}$] |
| $m$ | intermediate term in the P model [–] |
| $K$ | effective Michaelis-Menten coefficient of Rubisco [Pa] |
| $K_C$ | Michaelis-Menten coefficient of Rubisco for carboxylation [Pa] |
| $K_O$ | Michaelis-Menten coefficient of Rubisco for oxygenation [Pa] |
| $O$ | partial pressure of oxygen [Pa] |
| pH | measure of acidity: minus log (hydrogen ion concentration) [–] |
| $Q_{10}$ | ratio of reaction rate at temperature $T$ + 10 K to reaction rate at temperature $T$ [–] |
| $R$ | universal gas constant [J $mol^{-1}$ $K^{-1}$] |
| $R^2$ | coefficient of determination [–] |
| $T$ | absolute temperature [K] |
| $T_C$ | Celsius temperature [˚C] |
| $u^2$ | standard uncertainty |
| $V_{cmax}$ | maximum velocity of carboxylation (FvCB model) [µmol $m^{-2}$ $s^{-1}$] |
| β | ratio of cost factors for carboxylation and transpiration (P model) [–] |
| | $\gamma_{age}$ regression coefficient for the logarithm of forest stand age in years |
| | $\gamma_{Ppn}$ regression coefficient for mean annual precipitation |
| Γ* | $CO_2$ compensation point in the absence of mitochondrial respiration (FvCB model) [Pa] |
| $\delta^{13}C$ | normalized ratio of the stable carbon isotopes $^{13}C$ and $^{12}C$ relative to a standard reference [‰] |
| $\Delta H_{\Gamma*}$ | activation energy of Γ* [kJ $mol^{-1}$] |
| $\Delta H_{K\_C}$ | activation energy of $K_C$ [kJ $mol^{-1}$] |
| $\Delta H_{K\_O}$ | activation energy of $K_O$ [kJ $mol^{-1}$] |
| η* | viscosity of water relative to its value at 25˚C [–] |
| Θ | curvature parameter in the relation between electron transport and absorbed PPFD (FvCB model) [–] |
| ξ | stomatal sensitivity parameter (P model) [$kPa^{0.5}$] |
| $\phi_0(C_3)$ | intrinsic quantum efficiency of $C_3$ photosynthesis [–] |
| $\phi_0(C_4)$ | intrinsic quantum efficiency of $C_4$ photosynthesis [–] |
| χ | ratio of leaf-internal to ambient carbon dioxide [–] |
| $\partial f(x_i)/\partial x_i$ | sensitivity of GPP to variable $x_i$ |

# CHAPTER 1 BACKGROUND OF THE DOCUMENT

## 1.1. SCOPE AND OBJECTIVES

The TerrA-P project aims to implement and validate a new global monitoring system for primary production by land ecosystems. The project focuses on gross primary production (GPP) and above-ground biomass production (ABP), defined as follows:

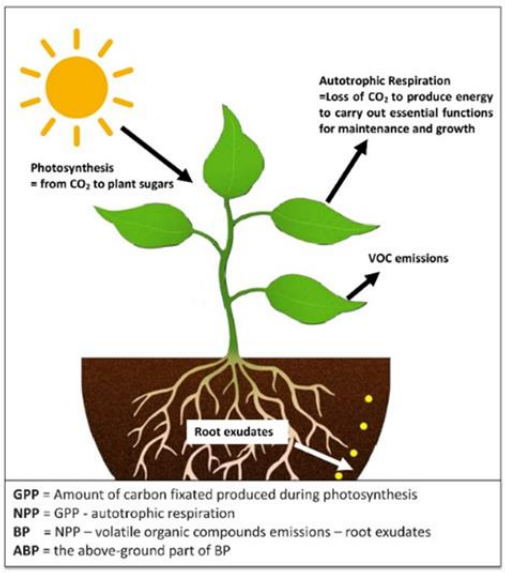


**Gross primary production** is the rate of total carbon fixation (photosynthesis) by the ecosystem. This is the most fundamental measure of primary production, as all other ecosystem functions depend on it. Also, thanks to the availability of eddy-covariance flux measurements, GPP data are available – at time scales from half-hourly up to multi-annual – for some hundreds of locations worldwide (albeit with a bias towards temperate regions), and for croplands as well as for natural and managed ecosystems.

*Figure 1 (left): schematic illustrating the different aspects of primary production.*

**Above-ground biomass production** is the rate of production of plant matter, excluding roots. This is a practically important measure, because this is the production rate of forage for grazing animals; it is closely related to the production rate of timber for harvest; and it can be converted (through data on the harvest index – the ratio of harvestable yield to ABP – for different crops) to estimates of crop yield. There are data on ABP, occasionally at a monthly time scale but more commonly at the annual time scale, for many ecosystems, especially crops and managed forests but also for natural ecosystems.

We chose not to focus either on (total) biomass production or on net primary production (NPP), for the following reasons:

**Biomass production** is the total rate of production of plant matter, including roots. For most crops the root production is of less interest than the above-ground production. Even for root crops there are data on the harvest index, so ABP can be used to predict harvestable yield by a simple conversion. There are some data on BP but in most cases the root production has not been measured directly, but rather inferred from above-ground measurements. Inevitably this increases the uncertainty of BP data.

**Net primary production** is defined as the difference between GPP and plant respiration. Formerly, NPP was assumed to equivalent to BP. Most data that claim to be NPP are, in fact, BP. But it is now

understood that a fraction of NPP – under some circumstances this can be as much as 20% – is "lost" from the plant by other pathways than respiration, in the form of volatile organic compounds (such as isoprene and monoterpenes) and/or root exudates, which do not contribute to biomass production. Moreover, most published data sets of "NPP" are of poor quality.

The aims of the project will be achieved by using spectral reflectance data from Sentinel-3 as input to a recently developed universal, first-principles light use efficiency (LUE) model for GPP, called the 'P' model (for 'production'). Initial calibration was carried out (and reported in ATBD v1) against GPP data derived from eddy-covariance carbon dioxide ($CO_2$) flux measurements at 17 selected sites. This calibration used a merged data set from SeaWiFS and MERIS (Global Vegetation Index, GVI) to provide the fraction of incident photosynthetically active radiation that is absorbed by green tissues (fAPAR), a key input to the P model. The model also requires meteorological data, all of which were derived for the initial calibration from direct measurements at the flux sites. The updated calibration presented in ATBD v2.1 (and shown here) is based on the same fAPAR data, but remotely sensed land surface temperature (LST) data from the Advanced Along-Track Scanning Radiometer (AASTR) were used to provide the temperature and vapour pressure deficit drivers for modelled photosynthesis. This substitution is desirable theoretically, because LST is expected to be closer to the actual temperature of leaves; and practically for the global application, because remotely sensed LST is retrieved at a higher spatial resolution than can realistically be achieved by interpolation of weather-station or meteorological analysis data.

The project has developed a prototype processing chain for 10-daily GPP and annual ABP by $C_3$ and $C_4$ plants. This includes data quality flags and a specification of per-pixel uncertainties, which has been implemented in the creation of model outputs for validation. Validation of the model is described in a separate document led by the University of Antwerp group. Validation was based on a more extensive data set of GPP, derived from eddy-covariance flux measurements in different biomes and climatic regions.

Annual ABP is derived from annual totals of GPP by applying functions decribing the above-ground production efficiency (ABPE), i.e. the ratio of annual ABP to annual GPP. This approach makes it possible to account for the large differences in ABPE between forests, non-forest ecosystems and crops, the effects of management, and the effect of forest stand age. This version of the ATBD (2.2) describes the derivation of these functions, based on data from sites where independent measurements of ABP and GPP were available. The ABP scheme (comprising the GPP model and the ABPE functions) will be validated by comparison to the most comprehensive available global set of quality-controlled data on annual ABP, compiled by the University of Antwerp group.

### 1.2. CONTENT OF THE DOCUMENT

- **Chapter 1** describes the background of the document.
- **Chapter 2** describes the criteria adopted for new primary production data products, taking into account both the requirements articulated by users, and scientific considerations.
- **Chapter 3** is a selective review of existing approaches to monitoring primary production from space, including those currently used operationally.
- **Chapter 4** describes the P model and the proposed manner of its implementation, including the approach used to calculate uncertainties; introduces the GPP calibration data set; presents the results of the ATBD v2.1 calibration; and demonstrates the application of the Copernicus Soil Water Index to modify the GPP product. This chapter also summarizes the statistical derivation of the functions for ABPE.
- **Chapter 5** summarizes the approach to validation and benchmarking.

# CHAPTER 2 CRITERIA FOR NEW PRIMARY PRODUCTION DATA PRODUCTS

## 2.1. INTERPRETATION OF USER REQUIREMENTS

TerrA-P has conducted a survey targeting various potential users of the proposed new products, including current users of the Copernicus Global Land Operations Lot1 (CGLOPS-1) of the Copernicus Global Land Service. The full details of the survey are described in the Requirements Baseline Document. It yielded the following key information for product design.

The *principal products currently in use* are MODIS GPP and net primary production (NPP), CGLOPS-1 dry matter production (DMP) products, and models. The new products should aim to reproduce (at least) the functionality of these existing, widely-used products.

Different users work at different *geographic scales*, from subnational to global. The new products should accordingly be global, gridded products allowing flexibility of application.

About three-quarters of users surveyed agreed with the proposed strategy to *focus on GPP* and *ABP*. Some caveats were mentioned, including the fact that GPP cannot be directly derived from flux measurements (ecosystem respiration has to be factored out through a 'partitioning' method, of which there are several that give somewhat different results); and the fact that total biomass production (including production below ground) may sometimes be of greater interest than ABP. We propose to deal with uncertainty in partitioning by using the range of alternative partitioning methods as a measure of uncertainty in observed GPP. For biomass production, however, the paucity and low reliability of data on below-ground production argues for maintaining a focus on ABP. We note that ABP is quantitatively related to below-ground production by, for example, root crops just as it is quantitatively related to above-ground production by grain crops.

Users were approximately equally divided in their preferences for *units of dry matter versus carbon*. For maximum comparability with existing products, and with the main data sources for each quantity, we propose supplying GPP in carbon units and ABP in dry matter units. Climate modellers preferred carbon units, but are likely to be more interested in 10-daily GPP than annual ABP.

Most users saw the need to consider *$C_3$ versus $C_4$ photosynthesis* but, not surprisingly, there was no specific proposal as to how the prevalence of the two pathways could be specified on a per-pixel basis. We propose to circumvent this problem by providing both as alternatives for every pixel.

Most users asked for a *data quality layer*, and *information on uncertainty*. A per-pixel uncertainty layer was not explicitly requested. However, a numbers of users in different ways indicated a need for quantitative, per-pixel uncertainty information. In our view a systematic approach to per-pixel uncertainty should be a significant part of product development, and would satisfy this need.

The most popular *sampling frequency* was 10-daily. A number of users voted for daily, but daily data on spectral reflectances are not meaningful because many dates, in most locations, will be affected by clouds. This problem can be largely circumvented by providing 10-daily composites. Most users asked for *data availability* in near-real time, that is, 3 to 5 days after acquisition.

The preferred *spatial resolution* is 300 m. Some users work with coarser resolutions which, however, can be readily obtained by post-processing of a 300 m product.

The average request in terms of *relative accuracy* was close to 20%, which likely provides a realistic target accuracy for both 10-daily GPP and annual ABP.

Table 1 summarizes the user requirements, and the specifications adopted that are consistent with these requirements as far as is technically feasible.

*Table 1: Summary of user requirements and specifications adopted for TerrA-P products.*

| **User requirement** | **Specification adopted** |
|---|---|
| Geographic scale subnational to global | Global gridded product |
| Focus on GPP and ABP | Focus on GBP and ABP |
| Carbon or dry-matter units | Carbon for GPP, dry matter for ABP |
| Distinction of $C_3$ and $C_4$ photosynthesis | Provide results for both $C_3$ and $C_4$ plants |
| Data quality layer, information on uncertainty | Provide per-pixel uncertainty estimates |
| Daily to 10-daily sampling frequency | 10-daily sampling frequency |
| Data availability in near-real time | Data available 3-5 days after acquisition |
| Spatial resolution 300 m or coarser | 300 m grid with facility for post-processing |
| Relative accuracy ca 20% | Target relative accuracy 20% |

## 2.2. SCIENTIFIC REQUIREMENTS

*A priori* we determined that new products should as far as possible possible satisfy a number of additional criteria, summarized here. These requirements go significantly beyond the current state of the art in LUE-based modelling.

*Explicit relationship to the standard model of photosynthesis*. The Farquhar, von Caemmerer and Berry (1980) (FvCB) model is the standard model of $C_3$ photosynthesis (von Caemmerer, 2000), and modifications exist to describe $C_4$ photosynthesis. There are thousands of published field measurements of the parameters defined in the FcVB model. All current ecophysiological theory, and the great majority of biophysical land-surface schemes for climate modelling, make use of the FvCB model. Therefore, a newly developed remotely sensed GPP product should be explicitly defined in terms of the FvCB model.

There is no such general model for plant respiration and other carbon "losses" from GPP. Thus models for biomass production should be based on GPP, with modifications to account for these losses as fractions of GPP.

*Representation of physiological effects of $CO_2$*. Models based on remotely sensed data, including those in operational use, generally do not consider the effect of changing atmospheric $CO_2$ concentration on the LUE of photosynthesis. Thus, they only consider a $CO_2$ effect in so far as it is manifested by changes in foliage cover that can be seen from space. As a direct consequence, products such as MODIS GPP and NPP severely underestimate the generally increasing trend in primary production due to rising $CO_2$ (De Kauwe et al., 2016a). Newly developed products should explicitly include the effect of $CO_2$ concentration on LUE.

*No discontinuities at biome boundaries*. Although the convention of defining different model parameter values per biome is entrenched in remote sensing applications, it inevitably leads to discontinuities at boundaries defined by an external classification. This is a highly undesirable property, because biomes intergrade. Imposed biome boundaries are arbitrary and differently

located according to different land cover products. New products should attempt to avoid such discontinuities.

*A demonstrated level of accuracy assessed by comparison to relevant measurements*. Eddy-covariance measurements of $CO_2$ flux can be processed ('partitioned') to yield estimates of daily, 10-daily, monthly or annual GPP. Flux measurement sites vary in public availability status, and in the length of records. Some sites are more suitable than others for model calibration and validation, because in areas of complex terrain or land use patterns there can be a severe problem in attempting to match remotely sensed spectral reflectance data with the (time-varying) footprint of the flux tower. Thus, model calibration and validation should be based on an informed selection of flux measurement sites.

# CHAPTER 3 REVIEW OF SELECTED EXISTING APPROACHES

## 3.1. BACKGROUND AND HISTORY

The basis for nearly all algorithms designed to calculate primary production based on remotely sensed data is the general LUE model first proposed by Monteith (1972, 1977). Monteith based this model on field measurements of crop growth in both tropical and temperate climates, showing that growth is proportional to the time-integral of the light absorbed by the crop.

The general LUE model can be applied either to GPP or to NPP. More formally, in a remote sensing context, the general LUE model states that primary production is proportional to the product of incident photosynthetic photon flux density (PPFD) and fractional green vegetation cover, also called fractional absorbed photosynthetically active radiation (fAPAR or FPAR). fAPAR depends on Leaf Area Index (LAI) but is closer to actual reflectance measurements than LAI, and more directly related to primary production. In the remote sensing literature, incident PPFD (μmol $m^{-2}$ $s^{-1}$) is more often described as 'incident photosynthetically active radiation' (IPAR) (W $m^{-2}$). The former term is more accurate because photosynthesis depends on the *number* of photons absorbed, rather than their energy (which varies with their wavelength). However, the two units can be interconverted, if it is assumed that the solar spectrum is constant.

NPP is the remainder of GPP after autotrophic (plant) respiration has converted approximately half of GPP back to $CO_2$. Traditionally, NPP has been regarded as synonymous with biomass production, i.e. the production of plant tissues. However, it is now recognized that a fraction (which can be as much as 20%) of NPP is lost from plants in the form of exudation from roots (a carbon subsidy to microbes in the rhizosphere, which enables plants to increase their uptake of soil nutrients) and emissions of volatile organic compounds (VOCs) such as isoprene and monoterpenes from leaves (which confer protection against both oxidants, including ozone, and high leaf temperatures). We therefore make a distinction between NPP and biomass production. The latter is of greater interest than NPP *sensu stricto* to users in forestry and agriculture.

Pioneering examples of remotely sensed primary production models are the Simple Diagnostic Biosphere Model (SDBM) of Knorr and Heimann (1995), the Carnegie-Ames-Stanford Approach (CASA) model of Potter et al. (1993), and the Global Production Efficiency Model (GLO-PEM) of Prince and Goward (1995). These models used spectral reflectance data from the Advanced Very High Resolution Radiometer (AVHRR) to infer fAPAR. A constant maximum LUE was specified, then reduced by scalars representing aspects of temperature and moisture conditions that can reduce LUE. The SDBM was combined with an atmospheric tracer transport model and deployed in an inverse mode, using observations of the seasonal cycle of atmospheric $CO_2$ concentration at different latitudes to estimate a single global maximum value for the LUE of NPP, and a single global $Q_{10}$ value to quantify the dependence of soil organic matter decomposition on temperature. In GLO-PEM, theoretical maximum LUE values for GPP were determined based on the FvCB model. One value was assigned for $C_3$ plants and another for $C_4$ plants. These values were modified following the FvCB model's estimation of photorespiratory carbon loss as a function of temperature. GLO-PEM also made use of a number of other remote-sensing approaches to estimate meteorological variables, including IPAR. Unusually, this modelling approach – further developed by Goetz et al. (1999) – aimed to derive all required meteorological and biophysical variables from remotely sensed platforms.

The Physiological Principles Predicting Growth (3-PG) model of Landsberg and Waring (1997) is also an LUE model and can be driven by remotely sensed and meteorological data. This model, focused on forest production, makes a number of empirically well-supported simplifications to predict GPP, NPP and forest growth.

All of the models discussed so far included an estimate of soil moisture availability as one of the factors reducing LUE.

In the following subsections, we review the principal literature on LUE models and note the key features of various widely used models, including those used operationally, and some other models that have introduced potentially useful innovations.

### 3.2. THE MODIS GPP AND NPP PRODUCTS

By far the most widely used remotely sensed primary production data products for scientific applications today are the MODIS GPP and NPP (MOD17) products (Running et al., 2004; Zhao et al., 2005). The most recent (2015) user's guide to the MOD17 products can be found at: http://www.ntsg.umt.edu/sites/ntsg.umt.edu/files/modis/MOD17UsersGuide2015_v3.pdf
MODIS GPP specifies a maximum LUE which varies per biome. This value is multiplied by two scalars formulated as ramp functions: a linearly declining function of daily vapour pressure deficit (vpd), between biome-specific limit values where the function equals one or zero, and a linearly increasing function of daily minimum temperature, between biome-specific limit values where the function equals zero or one. Soil moisture effects are not considered: thus implicitly, soil moisture effects are considered to be accounted for in the remotely sensed fAPAR, and/or the effect of vpd on photosynthesis. The calculations make use of a land-cover classification and a Biome Parameter Look-Up Table (BPLUT) which recognizes 10 biomes. The required meteorological data, including IPAR (incoming solar shortwave radiation multiplied by 0.45), are supplied by the Global Modeling and Assimilation Office (GMAO) of the US National Aeronautics and Space Administration (NASA) at a $1^{\circ} \times 1.25^{\circ}$ grid resolution. These data are smoothly interpolated to the finer (1 km) spatial resolution of the remotely sensed fAPAR data. The spatial and temporal resolution (8 days) of the product are set by the fAPAR data, which are obtained from the MODIS FPAR/LAI product.

Biome-specific model parameter values for MODIS GPP were based on literature-derived estimates used in the process-based BIOME-Biogeochemical Cycles model (BIOME-BGC: Running and Hunt, 1993). Thus, $CO_2$ flux data were not used in the initial calibration of the remote-sensing based model. However, the MODIS GPP product has been very extensively and independently evaluated by comparison with GPP derived from flux measurements. A number of these evaluation studies are cited in the user guide. Verma et al. (2014) included MODIS GPP – and also a version called MOD17-Tower, which was pre-calibrated against flux measurements – in a systematic global comparison with flux data-derived GPP. MODIS GPP was included in the set of seven LUE models compared globally with flux data-derived GPP by Yuan et al. (2014). Tang et al. (2015) undertook a comprehensive evaluation of MODIS GPP against flux data-derived GPP for forest ecosystems. Tagesson et al. (2017) showed that MODIS GPP greatly underestimates flux data-derived GPP in the Sahel, apparently due to unrealistically low maximum LUE assigned to semi-arid ecosystems.

The approach taken in the MODIS NPP product to derive NPP from GPP relies on separately modelling autotrophic respiration, which is separated into maintenance and growth components. NPP is then the difference between modelled GPP and modelled total autotrophic respiration. Maintenance respiration in the model depends on leaf area index (LAI), obtained from the MODIS FPAR/LAI product, and biome-specific values of specific leaf area, the ratio of fine root mass to leaf mass, base

maintenance respiration rates for leaves and fine roots, and a $Q_{10}$ value that specifies the steepness of an assumed exponential relationship to temperature. In the current version of MODIS NPP, the $Q_{10}$ of leaf maintenance respiration is a decreasing function of growth temperature. This is said to reflect respiratory acclimation, although Medlyn (2011) pointed out that the use of this function in fact further steepens the modelled negative response of NPP to temperature. Other components of maintenance respiration assume a fixed $Q_{10}$. Additional biome-specific information is used to infer annual growth respiration, which is then combined with annually integrated estimates of GPP and autotrophic respiration to yield annual NPP. Evaluation of NPP is considerably more difficult than evaluation of GPP, as the available data are far more limited. A number of compilations of annual NPP measurements have been made, however, and these have been used as a benchmark for MODIS NPP.

The MODIS GPP and NPP products were the first global and widely disseminated products of their kind. They represented a major technical advance, and now underpin a large number of high-profile scientific publications. However, criticisms have been made of some recent studies in which key assumptions underlying these products were overlooked. The study by Zhao and Running (2010) for example was criticized by Samanta et al. (2011) and Medlyn (2011), as the decline in NPP during the 2000 to 2009 period reported by Zhao and Running (2010) was not present in the remotely sensed data. It was, instead, a consequence of the high sensitivity of maintenance respiration to temperature in the model. Prentice (2013) noted that this sensitivity must be too high, because the interannual variability of MODIS NPP is so large as to fully account for the observed year-to-year variability of the atmospheric $CO_2$ growth rate – allowing no room for the effect of temperature variability on the soil decomposition rate, which is generally understood to be the key factor modulating the $CO_2$ growth rate (e.g. Wenzel et al., 2014).

Another emerging problem is the weak increase over time shown in the MODIS GPP and NPP products. This weak trend contrasts with the strong increases shown by most process-based models (Anav et al., 2015), the attribution of increasing measured GPP at flux sites to rising $CO_2$ (Fernández-Martínez et al., 2017), and the evidence for increasing LUE as the principal driver of a large amplification of the high-latitude seasonal cycle of atmospheric $CO_2$ (Graven et al., 2013; Wenzel et al., 2016; Thomas et al., 2017).

In process-based models, GPP and NPP increase primarily as a consequence of the rising atmospheric $CO_2$ concentration. Smith et al. (2016) asserted that process-based models overestimate the stimulatory effect of rising $CO_2$ concentrations on NPP. They reached this conclusion by comparing process-based model outputs with the much weaker trend shown by MODIS NPP. However, MODIS GPP and NPP do not allow $CO_2$ concentration to influence LUE; therefore, the only possible $CO_2$ influence in these models is via increasing fAPAR. There is a worldwide 'greening' trend which has been attributed in part to the effect of $CO_2$ in increasing NPP and water use efficiency (Donohue et al., 2013; Ukkola et al., 2015; Zhu et al., 2016). But Free Air Carbon Enrichment (FACE) experiments have shown that the principal effect of enhanced $CO_2$ on primary production in forests is through increased LUE, whereas increased LAI or fAPAR are much less important. Thus, the discrepancy noted by Smith et al. (2016) does not mean that process-based models overestimate the effect of $CO_2$ on NPP. Instead it means that MODIS NPP underestimates this effect (De Kauwe et al., 2016a), as a consequence of its design.

### 3.3. C-FIX AND THE DRY MATTER PRODUCTIVITY PRODUCT

Veroustraete et al. (1994, 2002) introduced the C-Fix model, a pioneer effort and the forerunner of the present-day Dry Matter Productivity (DMP) algorithm (Swinnen et al., 2015) currently provided

by CGLOPS1. The original version of C-Fix was a LUE model for GPP in which a maximum LUE (a single global value) was reduced through multiplication by scalars representing the effects of suboptimal temperature and water availability. Values for NPP were obtained from GPP using an empirical linear function of temperature to account for the fraction of GPP lost to autotrophic respiration.

C-Fix also included an attempt to account for an effect of rising atmospheric $CO_2$ concentration on photosynthesis via the FvCB model. However, the effect was implemented by way of the $CO_2$-dependence of the Rubisco-limited rate of photosynthesis, which is nearly always the rate that is measured when leaves are subjected to saturating light intensity (De Kauwe et al., 2016b). This rate depends steeply on $CO_2$. But it is not the rate actually realized in the field, at lower average light intensity. Under typical daytime field conditions the light- and Rubisco-limited rates are approximately equal (Maire et al., 2012). The light-limited rate depends on $CO_2$ as well, but less steeply than the Rubisco-limited rate. The original $CO_2$ response function in C-Fix therefore presumably overestimates the effect of $CO_2$ on GPP. However this overestimation may be tempered by the fact that no distinction is made between leaf-internal and ambient $CO_2$. The steepness of the response is thereby less than it would have been if leaf-internal $CO_2$ had been used.

Another limitation of C-Fix is its assumption of a universal, strongly peaked response of GPP to temperature with an optimum around 22˚C – thus not accounting for thermal acclimation, and necessarily underestimating GPP in hot climates. But C-Fix was designed for use in temperate forests and has in fact only been applied in temperate regions. Veroustraete et al. (2002) successfully compared C-Fix GPP predictions with flux data from forests in different regions of Europe.

C-Fix was not deployed operationally, but it provided the initial basis for the present operational DMP product (Swinnen et al., 2015). In DMP, IPAR is determined from solar shortwave radiation by applying a factor 0.48, and APAR is obtained by multiplying IPAR by a remotely sensed estimate of fAPAR, as in other models. Daily meteorological data supplied by the European Centre for Medium range Weather Forecasts (ECMWF) on a 0.25˚ grid are bilinearly interpolated to the remote-sensing pixels. A single global maximum value is assigned to the maximum LUE. This is modified by a temperature function and (for NPP) a further temperature function. These two functions are unchanged from C-Fix. Production is therefore likely to be underestimated in hot climates, due to the 'temperate' location of the peak of the temperature response function for LUE. There is no effect of water availability (apart from that manifested in changes in fAPAR) and the $CO_2$ response of C-Fix is not implemented. $C_4$ photosynthesis is not distinguished.

### 3.4. SOME RECENT DEVELOPMENTS AND TRENDS

Numerous LUE models have been developed in recent years with the expressed intention of achieving improved consistency with $CO_2$ flux-based measurements of GPP. These measurements, when suitably analysed, can provide more information about the controls of LUE than is utilized in an 'end-of-pipe' comparison of modelled and measured values of GPP.

The EC-LUE model (Yuan et al., 2007) requires only four quantities as input: fAPAR (which is estimated from the Normalized Difference Vegetation Index, NDVI), IPAR, air temperature and the Bowen ratio, which was inferred from other remotely sensed measurements (Yuan et al., 2007). In a later version the Bowen ratio was replaced by the ratio of actual evapotranspiration to net radiation (Yuan et al., 2010), which proved to be more robustly estimated than the Bowen ratio. EC-LUE has the merit of simplicity, as well as outperforming MODIS GPP in comparisons with flux measurements.

Further innovations in recent LUE models include consideration of seasonal variations in maximum LUE (Garbulsky et al., 2010; Lin et al., 2017), accounting for thermal acclimation (McCallum et al., 2013), the inclusion of an effect of diffuse light fraction on LUE (Donohue et al., 2014), and the use of a MODIS canopy conductance product to include effects of vpd and soil moisture availability (Yebra et al., 2015).

These various recent model developments differ in the extent to which they achieve good empirical results by increasing complexity and adding to the number of unknown parameters, *versus* the alternative of trying to make modelling more robust through the application of theory that can often simplify models and reduce the number of unknown parameters. McCallum et al. (2009), for example, argued for the inclusion of all of those processes that have been shown to improve model performance. An opposite view (Prentice et al., 2015) is that this is a flawed approach that tends always to increase uncertainty, rather than to reduce it, as the number of parameters increases and the transparency of the model decreases.

### 3.5. THE SCARF MODEL

Ogutu et al. (2013) introduced the Southampton Carbon Flux (SCARF) model, a new LUE model with a number of specific advantages for potential operational use. First, the remote sensing data used to drive the model are the MERIS Total Chlorophyll Index (MTCI). MTCI was considered by Ogutu et al. (2013) to offer an improvement over more standard 'greenness' measures as it explicitly relates to the abundance of green, photosynthesizing tissues. They argued that other measures of fAPAR used in LUE models include light absorption by non-green tissues that do not contribute to GPP. Second, the model substantially avoids spatial discontinuities and the use of a look-up table for biome-specific parameters by (a) adopting universal intrinsic quantum efficiency values defined in terms of the FvCB model for $C_3$ and $C_4$ plants respectively, and (b) applying universal temperature and $CO_2$ response functions for $C_3$ plants, and vpd response functions for $C_3$ and $C_4$ plants. The $CO_2$ and temperature response functions for $C_3$ plants were derived from the FcVB model, but an empirical formulation was used for the vpd response functions. A look-up table (together with a number of simplifying assumptions) was used to estimate the fraction of $C_3$ versus $C_4$ photosynthesis on a per-pixel basis. The model was evaluated successfully against GPP data derived from flux measurements across Europe and the USA.

Ogutu and Dash (2013) showed that the fidelity of flux measurements to the FvCB model at two study sites was close enough that reasonable estimates of 'green' fAPAR could be obtained by inversion of the model, i.e. estimating the fAPAR required to produce the observed patterns of GPP. This finding strongly supports the notion that LUE models could avoid the need for multiple unknown parameters (including the need for look-up tables for vegetation types, apart from the issue of $C_3$ versus $C_4$ photosynthesis) through application of the FvCB model.

### 3.6. THE BESS MODEL

The Breathing Earth System Simulator (BESS) by Ryu et al. (2011) represents an advanced modelling system for GPP and evapotranspiration (ET) and included many novel features. The model was designed to be the 'first system that harmonizes and utilizes MODIS Atmosphere and Land products on the same projection and spatial resolution over the global land' (Ryu et al., 2011, p. 1), thereby utilizing remotely sensed solar radiation and other meteorological data (from MODIS) and avoiding the need to interpolate such data from a coarse spatial grid. The model was described as calibration-free, that is, no parameters were to be estimated from flux data; all were to be specified

independently. A global selection of 33 flux measurement sites was used to independently evaluate the model's predictions of both GPP and ET.

BESS is more complex than any of the other models discussed in this review. It includes an explicit radiative transfer model for solar radiation in the canopy; a 'two-leaf' model that distinguishes the properties of sun and shade leaves, which has been claimed to provide better accuracy, especially in modelling the differential penetration of diffuse versus direct light into the canopy and the consequences for photosynthesis; consideration of foliar clumping effects on photosynthetic light absorption (making use of a satellite-derived foliar clumping index product); and an extended FvCB model, including light-, Rubisco- and triose phosphate utilization-limited rates of photosynthesis. However, this complexity comes at a considerable cost, both computational, and in terms of data availability.

The model was set up on the Microsoft Azure cloud computing system, as it was considered to be infeasible on the supercomputing resources available at Berkeley. Many compromises were unavoidably made. A look-up table was used to provide values of many parameters, including the carboxylation capacity ($V_{cmax}$) over much of the Earth's surface. For some biomes $V_{cmax}$ was estimated from foliage N, which in turn was estimated from vegetation albedo – this approach relying on the (questionable) relationship between foliar N and $V_{cmax.}$ The ratio of leaf-internal to ambient $CO_2$ was set at constant values for $C_3$ and $C_4$ plants respectively, thus disregarding the well-established effect of vpd on this ratio. Some external data, not available from MODIS, were obtained from a coarsely gridded re-analysis product. Thus, although BESS includes many advanced features and the ideal of obtaining all required information from remote sensing remains worth pursuing, this ideal was not in fact realized. This approach does not appear to provide a useful way forward for the development of operational systems at the present time.

# CHAPTER 4 THE P MODEL: DESCRIPTION OF THE PROPOSED METHOD

## 4.1. THE P MODEL

The P model is fully derived and described by Wang et al. (2017a). Aspects of the underlying theory have been applied by Keenan et al. (2016), Wang et al. (2017b) and Smith et al. (in press). Unlike any of the LUE models discussed above, the P model possesses all of the following desirable attributes for a 'next-generation' primary production monitoring system:

- An explicit derivation from the FvCB model, and a clear relationship to a well-established functional form for stomatal behaviour – both elements required for a prediction of GPP.
- A representation of physiological $CO_2$ effects on photosynthesis that is consistent with both the FvCB model and results from FACE experiments.
- No distinctions among plant functional types and biomes (except for the difference between $C_3$ and $C_4$ plants), eliminating the need for spatial discontinuities induced by the use of a land-cover classification and look-up table.
- Demonstrated success in representing flux-derived GPP across different biomes at monthly time scales.

The model is extremely parameter-sparse, while achieving a fidelity to data comparable with or better than other models. This combination of simplicity with accuracy has been achieved through the development of theory that accounts for the observed environmental dependencies of the ratio (henceforth termed χ) of the leaf-internal ($c_i$) to ambient ($c_a$) partial pressures of $CO_2$ in $C_3$ plants; and the acclimation of photosynthetic parameters in space and time. Both aspects of the theory rely on eco-evolutionary optimality concepts to derive testable hypotheses, which in turn yield good agreement with observations from field measurements and field experiments.

### 4.1.1. PREDICTING χ WITH THE LEAST-COST HYPOTHESIS

Prentice et al. (2014) tested a quantitative theory based on a hypothesis first proposed by Wright et al. (2004), that plants should minimize the sum of the unit costs (per unit of carbon assimilation) of maintaining the capacities for carboxylation (proportional to $V_{cmax}$) and water transport (proportional to the maximum rate of transpiration). Transpiration is a requirement for photosynthesis because stomata have to open to allow $CO_2$ to diffuse towards the chloroplasts. In so doing, they draw water from the soil to replenish that lost by evaporation through the stomata. Prentice et al. (2014) showed that this 'least-cost' criterion leads to an optimal value of $\chi$ as a function of environmental variables (temperature and vpd) that is independent of PPFD and almost independent of $c_a$. This value is given by:

$$\chi = \Gamma^*/c_a + (1 - \Gamma^*/c_a)\,\xi/(\xi + \sqrt{D}), \quad (1a)$$

$$\xi = \sqrt{\{\beta(K + \Gamma^*)/1.6\eta^*\}} \quad (1b)$$

where $\Gamma^*$ and $K$ are respectively the photorespiratory compensation point and the effective Michaelis-Menten coefficient of Rubisco (both known functions of temperature and atmospheric pressure), β is an empirical constant (estimated from $\delta^{13}C$ data: Wang et al., 2017a), $\eta^*$ is the

viscosity of water relative to its value at 25˚C (a known function of temperature), and $D$ is the vpd. As $\Gamma^* << c_a$ under field conditions, and $K >> \Gamma^*$, equation (1) is well approximated by:

$$\chi = \xi/(\xi + \sqrt{D}) \quad (2a)$$

$$\xi = \sqrt{\{\beta K/1.6\eta^*\}} \quad (2b)$$

Equation (2a) is mathematically identical with the 'universal stomatal model' proposed by Medlyn et al. (2011) and tested against a globally distributed set of gas-exchange measurements by Lin et al. (2012). Lin et al. (2012) also showed that $\xi$ (there called $g_1$) increases approximately exponentially with temperature. This was predicted by Medlyn et al. (2011). It is also predicted by equation (2b), because of the strong temperature dependencies of both $K$ (increasing) and $\eta^*$ (decreasing).

Wang et al. (2017a, b) noted that the optimal value of $\chi$ should also depend on elevation, acting through the effects of changing atmospheric pressure on the partial pressures of both oxygen, which competes with $CO_2$ for the Rubisco catalytic sites, and water vapour. Wang et al. (2017a) used a large data set of leaf stable carbon isotope ($\delta^{13}C$) measurements to show that all three environmental dependencies are correctly predicted by the model. The predicted partial derivatives of $\ln \chi/(1 - \chi)$ are 0.055 $K^{-1}$ for temperature, –0.5 for ln vpd, and –0.08 $km^{-1}$ for elevation. These partial derivatives were independently estimated from the $\delta^{13}C$ data by multiple linear regression, yielding 95% confidence intervals that include the predicted values: (0.046, 0.058) for temperature, (–0.61, –0.48) for ln vpd, and (–0.13, –0.08) for elevation.

#### 4.1.2. PREDICTING GPP WITH THE CO-ORDINATION HYPOTHESIS

Wang et al. (2017a) also applied the co-ordination hypothesis, which proposes that acclimation (on time scales of weeks to months) should tend to equality of Rubisco- and light-limited photosynthetic rates. This long-standing idea is well supported by independent studies (Haxeltine and Prentice, 1996; Dewar, 1996; Maire et al., 2012; Togashi et al., 2018) and has a number of implications that are useful for modelling. These include a simple method to predict the spatial and temporal acclimation of $V_{cmax}$ as a function of IPAR and temperature, meaning that $V_{cmax}$ does not have to be specified independently (Smith et al., in press). A variant of this principle is already included in the widely used Lund-Potsdam-Jena (LPJ) dynamic global vegetation model (Sitch et al., 2003) and models derived from LPJ, including the LPX global carbon cycle model (Stocker et al., 2013), although its implications have not been much explored by the users of these models.

Wang et al. (2017a) further showed that a cost-benefit analysis of the maximum electron transport capacity $J_{max}$ – which can be measured in the field by artificially increasing $c_a$ to a high level – leads to a predictable optimal ratio of $J_{max}$ to $V_{cmax}$ that declines steeply with growth temperature, in accordance with experimental findings. The mathematical optimization was performed using the Smith formula relating the electron transport rate to absorbed light at the leaf level. Inclusion of this acclimation of $J_{max}$ has been found to exert a modest but significantly beneficial effect on the prediction of $V_{cmax}$. Closely similar results are found using the alternative empirical light response curve (a non-rectangular hyperbola with curvature parameter $\Theta$) that is more commonly used in conjunction with the FvCB model (Smith et al., in press). Regardless of which light-response curve is used, the practical consequence is the $J_{max}$, like $V_{cmax}$, does not need to be independently specified.

Together, the elements described above define a model to predict GPP. This is achieved simply by equating the light- and Rubisco-limited rates of photosynthesis in the FvCB model (implicitly over an acclimation period of days to weeks, compatible with the time scale of remotely sensed fAPAR products), and re-arranging to eliminate $\chi$, $V_{cmax}$ and $J_{max}$ (Wang et al., 2017a):

$$GPP = \phi_0(C_3) \times fAPAR \times IPAR \times m \sqrt{\{1 - (c^*/m)^{2/3}\}} \quad (3a)$$

where $\phi_0(C_3)$ is the dimensionless intrinsic quantum efficiency of $C_3$ photosynthesis (taken to be 0.085 by Wang et al., 2017a), $c^*$ is a parameter representing the unit cost of maintaining the capacity for electron transport, and

$$m = \{c_a - \Gamma^*\} / \{c_a + 2\Gamma^* + 3\Gamma^* \sqrt{[1.6\, \eta^*\, D\, \beta^{-1}\, (K + \Gamma^*)^{-1}]}\} \quad (3b)$$

Equation (3) has the mathematical form of a LUE model: that is, for a given set of environmental conditions (ambient atmospheric $CO_2$, temperature, atmospheric pressure and vpd) modelled GPP is proportional to the absorbed PPFD. But unlike other LUE models, equation (3) is now explicitly defined in terms of the FvCB model of photosynthesis. Although GPP at time scales of minutes to hours (as seen, for example, during the diurnal cycle of $CO_2$ flux) has a well-known *saturating* response to IPAR, GPP at longer (e.g. weekly) time scales has a *linear* response to IPAR, conferred by the acclimation of $V_{cmax}$. This principle was previously articulated by Haxeltine and Prentice (1996) and Dewar (1996), and provides a theoretical underpinning for LUE models (Medlyn, 1998). Equation (3) gives mathematical expression to the principle, and has proved to be at least as effective in terms of simulating flux-derived monthly GPP as other LUE models – as shown in Wang et al. (2017a), and in Table 2 below.

*Table 2: Goodness of fit ($R^2$) and root-mean-squared error of prediction (RMSE) statistics for P model (Wang et al., 2017a) predictions of monthly GPP, compared with results from several LUE models tested against flux measurements by Yuan et al. (2014).*

| | $R^2$ | | RMSE | |
|---|---|---|---|---|
| | This study | Yuan et al. | This study | Yuan et al. |
| All ecosystems | 0.551 | 0.553 ± 0.096 | 2.094 | 2.428 ± 0.275 |
| Shrubland | 0.772 | 0.255 ± 0.175 | 2.165 | 1.866 ± 0.915 |
| Deciduous broadleaf forest | 0.588 | 0.703 ± 0.094 | 2.766 | 2.919 ± 0.450 |
| Evergreen broadleaf forest | 0.341 | 0.119 ± 0.063 | 2.046 | 2.961 ± 0.801 |
| Evergreen needleleaf forest | 0.535 | 0.501 ± 0.108 | 1.856 | 2.384 ± 0.437 |
| Grassland | 0.572 | 0.631 ± 0.076 | 2.025 | 2.109 ± 0.280 |
| Mixed forest | 0.700 | 0.637 ± 0.068 | 1.824 | 2.339 ± 0.325 |

#### 4.1.3. EFFECTS OF $CO_2$ IN THE P MODEL

It follows from the co-ordination hypothesis that the benefit of rising $CO_2$ in increasing the LUE of GPP by $C_3$ plants will be limited to its effect on the *light-limited* rate of photosynthesis. This effect is predicted by the P model, with no additional parameter requirements, including its well-known interaction with temperature and vpd. Effects of $CO_2$ on different photosynthesis metrics, as measured in 12 FACE experiments, were the subject of a meta-analysis by Ainsworth and Long (2005). They showed (for an increase of approximately 200 ppm in $c_a$) that LUE changed by an average of +12 ± 9%, instantaneous water-use efficiency by +54 ± 17%, and stomatal conductance by –20 ± 3%. Corresponding predictions with the P model were +17%, +55% and –15% (Wang et al., 2017a).

#### 4.1.4. SOIL MOISTURE EFFECTS

In common with many LUE models, including those used operationally, the P model when driven by air temperature does not take account of soil moisture effects – except in so far as they are manifested through changes in fAPAR. In relatively moist soils the actual soil moisture content has little or no effect on LUE. Analysis of flux-based GPP measurements at most of the sites considered by Wang et al. (2017a), including a number of sites with pronounced dry seasons, has confirmed that there is no universal fall-off of LUE with drought. The implication is that drought-induced reduction of GPP is already accounted for through the response of fAPAR to drought.

However, some ecosystems (for example, some tropical savannas and Mediterranean forests) regularly show reduced LUE during part or all of the dry season (Stocker et al., 2018a). Moreover, extreme droughts to which ecosystems are not well adapted are expected to suppress LUE by a combination of reduced $\chi$ and (under the most severe drying) reduced $V_{cmax}$, as has been observed in drying-down experiments (Zhou et al., 2013). Therefore, in common with other operational products, the P model driven by air temperature is likely to overestimate dry-season GPP in some ecosystems, and to underestimate the negative effect of extreme droughts on GPP. These deficiencies could in principle be corrected through the use of a soil water index, in combination with the empirical functions presented by Stocker et al. (2018b), to modify the modelled GPP. When LST is used as a driver, however, the P model also implicitly takes account of the effect of restricted transpiration on LST. In this project, simulations driven by ECMWF air temperatures and by remotely sensed LST have both been conducted, and included in the validation protocol. This document also shows preliminary results using a soil water index as an additional input.

#### 4.1.5. $C_4$ PHOTOSYNTHESIS

The simplest way to implement $C_4$ photosynthesis makes just two modifications to equation (3). First, a generic $\phi_0$ value suitable for $C_4$ plants must be chosen (taken to be 0.055 in current work). Second, $c_a$ is made arbitrarily large. These two changes lead to a simplified equation for $C_4$ photosynthesis:

$$GPP = \phi_0(C_4) \times fAPAR \times IPAR \quad (4)$$

GPP of $C_4$ plants can benefit from rising $CO_2$ under conditions of limited water availability, because water-use efficiency increases even if photosynthesis does not. However, this benefit is expected to be fully realized in increasing fAPAR.

#### 4.1.6. MODELLING ABOVE-GROUND BIOMASS PRODUCTION

The translation from GPP to ABP (in carbon units, easily modified to dry matter units) can be summarized conceptually by the formula ABP = $(1 - f_{BG})$ x CUE x GPP, where $f_{BG}$ is the fraction of NPP allocated below ground (including root exudation, as well as allocation to the maintenance and turnover of roots) and CUE is the carbon use efficiency, i.e. the ratio of NPP to GPP. (This formula disregards the fraction of NPP allocated to VOC emission, which is much smaller than $f_{BG}$.)

The additional terms required to calculate ABP from GPP are, unfortunately, much less well understood from a theoretical and quantitative point of view than the terms in the equations for GPP itself. There are indications for two competing effects of temperature on ABPE. On the one hand, acclimation of $V_{cmax}$ results in a weakly increasing $V_{cmax}$ with growth temperature (Togashi et al., 2018); and leaf dark respiration varies approximately in proportion to $V_{cmax}$, according to the FvCB model. Accordingly, leaf dark respiration also shows a weak increase with growth temperature (Atkin

et al., 2015). This effect, by itself, would be expected to cause CUE to decrease with increasing temperature. On the other hand, warm conditions increase the availability of soil nutrients by enhancing the rates of microbial metabolism, thus diminishing the need for plants to allocate carbon below ground – thereby reducing $f_{BG}$ (Gill and Finzi, 2017), and potentially also increasing CUE. But there is no scientific consensus about the relative magnitudes of these effects, or indeed any other possible climatic effects on ABPE. Moreover, there is strong evidence that ABPE is influenced by non-climatic factors: soil fertility (Vicca et al., 2012), forest stand age and, above all, land management status (Campioli et al., 2015). Thus, a remotely sensed ABP product should not simply estimate ABP for a given pixel, but should provide users with alternative functions allowing land use (and in the case of forests, stand age) to be taken into consideration.

The general approach adopted here is to use available ecosystem carbon budget data (including independent measurements of GPP and ABP), at sites where land cover, land use and forests stand age are known, to derive such functions statistically. This approach is preferred to trying to model total autotrophic respiration, which has proved to be a major limitation of the MODIS NPP product, and below-ground allocation. Because of the ubiquitous acclimation of autotrophic respiration to temperature (Atkin et al., 2015), the instantaneous response of plant respiration rates to temperature (as expressed in the $Q_{10}$ factor employed by many models, including MODIS NPP) is actually irrelevant to the prediction of ABPE. In contrast, land cover/land use categories and forest stand age convey important information for determining ABPE.

## 4.2. DATA NEEDS TO IMPLEMENT THE P MODEL

Here we list the data needed for implementation of the P model, and the specific data sources that were used for calibration and validation.

- **Solar radiation and vapour pressure:** For calibration, in-situ measurements at the flux sites were used. For validation, the data were obtained from the ECMWF high-resolution forecast model. These data are operational forecasts for the next 24 hours, from the ERA-Interim reanalysis (Dee et al., 2011) for 1989-2008 and thereafter obtained via the MeteoGroup operational forecast system: see https://www.ecmwf.int/sites/default/files/elibrary/2015/16559-user-guide-ecmwf-forecast-products.pdf
  IPAR data were derived from global radiation and converted to PPFD for input to the P model using the conversion factor 2.04 µmol $J^{-1}$ (Meek et al. 1984). Vapour pressure deficit was calculated from vapour pressure and temperature by standard equations in Allen et al. (1998).
- **Temperature:** For calibration, daily temperature data were provided in ATBD v1 from in-situ air temperature measurements at the flux sites, and here from remotely sensed daytime LST. For validation, daily temperature data were provided from (a) ECMWF meteorological data, as described above for solar radiation and vapour pressure, and (b) again from remotely sensed daytime LST. The source of remotely sensed LST data was level 2 ENVISAT AATSR (Ghent et al., 2012) obtained via the ESA project Globtemperature (http://www.globtemperature.info/). Pre-processing of these data involved cloud/shadow masking and interpolation and smoothing (modified from Swets et al., 1999) to provide 10-daily averages.
- **fAPAR** data for calibration were obtained from SeaWiFS and MERIS GVI data (Ceccherini et al., 2013) via fapar.jrc.ec.europa.eu. For validation, fAPAR data were obtained from MERIS GVI (Gobron et al., 1999) via http://meriss10.vgt.vito.be.
- **Ambient partial pressure of $CO_2$**: the time-varying $CO_2$ mole fraction obtained from the monitoring station at Mauna Loa, Hawaii is converted to partial pressure units, and used as input

to the P model. Data are from the Scripps Institution $CO_2$ monitoring network (Keeling et al., 2001):
http://scrippsco2.ucsd.edu/data/atmospheric_co2/mlo

- **$C_3$ versus $C_4$ photosynthesis**: the need for data on the distribution of $C_3$ versus $C_4$ plants (which is problematic, especially where crops are concerned) is circumvented by providing both values for every pixel.
- **Soil moisture**: in an alternative P model version, we have used the Soil Water Index provided by the Copernicus Global Land Service: https://land.copernicus.eu/global/products/swi at 0.1˚ grid resolution (10-daily averages). The version SWI–060 with a characteristic time of 60 days was chosen, following Ceballos et al. (2005), as corresponding to a typical soil depth.

## 4.3. THE APPROACH TO ESTIMATING PER-PIXEL UNCERTAINTY IN GPP

The P model algorithm is derived from first principles and consists of a single equation, which can be differentiated with respect to all of the uncertain quantities that it contains. We have accordingly implemented a classical Type B uncertainty evaluation, which is derived analytically and produces a per-pixel uncertainty value explicitly considering the known sources of uncertainty in different quantities entering the model and combining them using established principles.

### 4.3.1. UNCERTAINTY EVALUATION BASED ON THE P MODEL ALGORITHM

Equations (3) and (4) contain a number of input variables and parameters whose uncertainty can be quantified. In addition, a number of the photosynthetic parameters are temperature-dependent. Uncertainties in the temperature dependencies are separated from uncertainty in the temperature data by applying the following standard formulae:

$$\Gamma^* = \Gamma^*[25] \exp\{(\Delta H_{\Gamma^*}/R)(1/298.15 - 1/T)\} \quad (5)$$

$$\eta^* = \exp\{580\,[1/(T - 138)] - [1/(160]\} \quad (6)$$

$$K = K_C\,(1 + O/K_O) \quad (7)$$

$$K_C = K_C[25] \exp\{(\Delta H_{K\_C}/R)(1/298.15 - 1/T)\} \quad (8)$$

$$K_O = K_O[25] \exp\{(\Delta H_{K\_O}/R)(1/298.15 - 1/T)\} \quad (9)$$

where $R$ is the universal gas constant (8.314 46 J mol$^{-1}$ K$^{-1}$), $T$ is the canopy temperature (K), $K_C$ is the Michaelis-Menten coefficient for carboxylation (Pa), $K_O$ is the Michaelis-Menten coefficient for oxygenation (Pa), $O$ is the partial pressure of oxygen (209 460 µmol mol$^{-1}$ x atmospheric pressure in Pa); $\Gamma^*[25]$, $K_C[25]$ and $K_O[25]$ are the values of $\Gamma^*$, $K_C$ and $K_O$, respectively, at 298.15 K; and $\Delta H_{\Gamma^*}$, $\Delta H_{K\_C}$ and $\Delta H_{K\_O}$ are the corresponding activation energies (J mol$^{-1}$). Moreover, if $D$ is estimated from absolute water vapour pressure ($e_a$) and saturation vapour pressure ($e_s$), then:

$$D = e_s(T_C) - e_a \quad (10)$$

where $e_s = e_s(0) \exp\{17.27\,T_C/(T_C + 237.3)\}$ (Pa) and $T_C = T - 273.15$ K.

Those quantities that are either defined precisely, or known with an uncertainty that is effectively negligible in this context, have been assigned numerical values above and will not be considered further. In the following section, we describe the approach that we have adopted in the validation

exercise to derive standard uncertainties for the remaining quantities. The formulation above allows each of the sources of uncertainty to be considered independent and, therefore, uncertainties from each source to be combined using the standard formula:

$$u^2(y) = \sum_i (\partial f/\partial x_i)^2 \, u^2(x_i) \quad (11)$$

where $u(y)$ is the standard uncertainty of GPP, $\partial f/\partial x_i$ is the sensitivity of GPP to variable $x_i$ (obtained by differentiating equation (3) with respect to each uncertain variable and evaluating the partial derivative at the current central value of $x_i$), and $u(x_i)$ is the standard uncertainty of $x_i$.

#### 4.3.2. DATA UNCERTAINTIES

**fAPAR**: standard uncertainties have been estimated as the standard deviation of values in the 9 x 9 pixel grid surrounding the pixel of interest.

**LST**: the data have been smoothed and gap-filled. Uncertainties provided on a per-pixel basis have been averaged over each dekad for each pixel.

**$CO_2$ mole fraction** data, obtained on an annual basis from the Scripps Institute of Oceanography Mauna Loa record, have been assigned a nominal uncertainty of ± 0.1 ppm. However, substantially greater uncertainty derives from local variations in $c_a$ due to ground-level sources and sinks in soils and vegetation, and local industrial and/or transport sources. This uncertainty was approximated as the difference between the current global value and the corresponding measured value at each of the flux sites. The total uncertainty ascribed to $CO_2$ was small, < 0.1%.

Uncertainties were not available for data on **shortwave radiation** or **vapour pressure**, and are not provided in the ECMWF operational data stream. However, we note that the calculation of vpd depends on LST and therefore the uncertainties in LST, at least, propagate into vpd.

In the global GPP product, uncertainties on fAPAR will eventually be derived from per-pixel uncertainties provided with the Sentinel-3 data. How to estimate uncertainties in the other meteorological variables remains to be considered.

*Parameter uncertainties*

The parameter **β** was estimated based on leaf $\delta^{13}C$ data, from the intercept of the regression of ln $\chi/(1-\chi)$ against environmental predictors (Wang et al., 2017a). The uncertainty of this estimate was assessed from the standard error of the intercept, and inflated to account for uncertainty in the conversion from stable isotope measurements to χ. The value used was β = 160 ± 2.7 (H. Wang, unpublished analysis).

The parameter ***c**** was estimated from published values of electron transport capacity ($J_{max}$) and carboxylation capacity ($V_{cmax}$) under a variety of experimental growth conditions (Kattge and Knorr, 2007; Wang et al., 2017a). The uncertainty of $c^*$ was estimated based on a regression of experimentally determined $J_{max}/V_{cmax}$ values against growth temperature. The value used was 0.41 ± 0.112 (H. Wang, unpublished analysis).

The remaining parameters of equations (3) and (4) are standard elements of the FcVB photosynthesis model. They are rather accurately measured, and show relatively little variation among different

plant species and measurement techniques. Nonetheless, they are subject to some uncertainty, which is taken into account as described below.

**$\phi_0(C_3)$ and $\phi_0(C_4)$**: published surveys of measurements on various species show some variability in these parameters (Skillman, 2008; Zhu et al., 2010), with an approximately normally distribution across species within each photosynthetic pathway. It is appopriate to calibrate these parameters within a plausible range, because of natural variation in their values across species; natural variation in the fraction of photosynthetically active radiation used for photosynthesis; and unresolved systematic variation in magnitude among different remotely sensed fAPAR products.

**$\Gamma^*[25]$, $K_C[25]$, $K_O[25]$ and the corresponding activation energies**: most recent modelling studies have used the *in vivo* values determined originally by Bernacchi et al. (2001), but other experimental data sets have given slightly different reference values and activation energies (De Kauwe et al., 2016b). There is also some variation in Rubisco kinetic properties across species from different environments (e.g. Hermida-Carerra et al., 2016). Based on this literature, we have adopted the following values (and uncertainties) for each parameter: $\Gamma^*[25]$ = 4.08 ± 0.10 Pa at standard atmospheric pressure; $\Delta H_{\Gamma^*}$ = 27055.67 ± 5020.93 J mol$^{-1}$; $K_C[25]$ = 40.41 ± 3.45 Pa; $\Delta H_{K\_C}$ = 64805.5 ± 5018.50 J mol$^{-1}$; $K_O[25]$ = 27480 Pa (no uncertainty assigned); $\Delta H_{K\_O}$ = 36164 ± 152.74 J mol$^{-1}$.

#### 4.3.3. COMBINING UNCERTAINTIES

Derivatives of equation (3) with respect to each uncertain quantity have been obtained analytically. For constant quantities, such as the two $\phi_0$ values, the derivative are pre-calculated. For quantities that vary in time and/or space, the derivative is evaluated as part of the standard workflow.

### 4.4. A PRELIMINARY CALIBRATION DATA SET FOR GPP

The University of Antwerp group has selected from the most recent synthesis data set (http://fluxnet.fluxdata.org/data/fluxnet2015-dataset/) 17 flux sites in different biomes that have data in the public domain, and are characterized by multi-year records (daily data over a period of at least 5 years) with good quality GPP data, checked by the standardized methodology defined by FLUXNET (Reichstein et al., 2005; Papale et al., 2006), and a large, relatively homogeneous vegetation footprint (at least 1 km x 1 km) to ensure reliable comparisons between *in situ* and remotely sensed data. These 17 sites (

Table 3) provide the basis for calibration.

Table 3: The calibration set of eddy-covariance flux measurement sites. VEG = IGBP vegetation type: EBF = evergreen broadleaf forest, ENF = evergreen needleleaf forest, OSH = open shrubland, CRO = cropland, DBF = deciduous broadleaf forest.

| CODE | NAME | LAT (˚) | LONG (˚) | ELEV (m) | VEG |
|---|---|---|---|---|---|
| AU-Tum | Tumbarumba | –35.6566 | 148.1517 | 645 | EBF |
| CA-NS3 | UCI-1964 burn site | 55.9117 | –98.3822 | 260 | ENF |
| CA-NS6 | UCI-1989 burn site | 55.9167 | –98.9644 | 244 | OSH |
| CA-Obs | Saskatchewan – Western Boreal, Mature Black Spruce | 53.9872 | –105.1178 | 629 | ENF |
| DE-Geb | Gebesee | 51.1001 | 10.9143 | 162 | CRO |
| DE-Hai | Hainich | 51.0792 | 10.4530 | 430 | DBF |
| DE-Kli | Klingenberg | 50.8929 | 13.5225 | 478 | CRO |
| FI-Hyy | Hyyttiälä | 61.8475 | 24.2950 | 181 | ENF |
| FR-Fon | Fontainebleau-Barbeau | 48.4764 | 2.7801 | 103 | DBF |
| FR-LBr | Le Bray (after 28 June 1998) | 44.7171 | –0.7693 | 61 | ENF |
| FR-Pue | Puechabon | 43.7414 | 3.5958 | 270 | EBF |
| IT-Cpz | Castelporziano | 41.7052 | 12.3761 | 68 | EBF |
| NL-Loo | Loobos | 52.1666 | 5.7436 | 25 | ENF |
| US-Ha1 | Harvard Forest EMS Tower (HFR1) | 42.5378 | –72.1715 | 340 | DBF |
| US-MMS | Morgan Monroe State Forest | 39.3232 | –86.4131 | 275 | DBF |
| US-UMB | University of Michigan Biological Station | 45.5598 | –84.7138 | 234 | DBF |
| US-WCr | Willow Creek | 45.8059 | –90.0799 | 520 | DBF |

## 4.5. CALIBRATION RESULTS

Simulations were set up for each of the calibration sites using local meteorological measurements of daily total incoming shortwave radiation and vapour pressure. Temperature was derived from remotely sensed LST, and vapour pressure was converted to vpd using the standard method (Allen et al. 1998) using LST as the relevant temperature for saturation vapour pressure. Annual values of $CO_2$ were prescribed. Low-temperature inhibition of photosynthesis was represented in the simplest possible way, by setting GPP to zero during periods with subfreezing temperatures.

$\phi_0(C_3)$ was estimated from the comparison of P model estimates with the GPP data by varying its value in the model between 0.05 and 0.1125. The optimized value (yielding the smallest sum of RMSE across sites) obtained in the initial calibration (ATBD v1) was 0.084: only marginally different from the value of 0.085 adopted in Wang et al. (2017a). The updated calibration presented here, with temperature provided by LST, yielded an optimized value of 0.092, which is still well within the experimentally observed range based on leaf-level measurements, and closer to the typical value of 0.096 provided by Skillman (2008). Figure 2 shows the effect of varying $\phi_0(C_3)$ on the sum of RMSE across sites in the updated calibration.

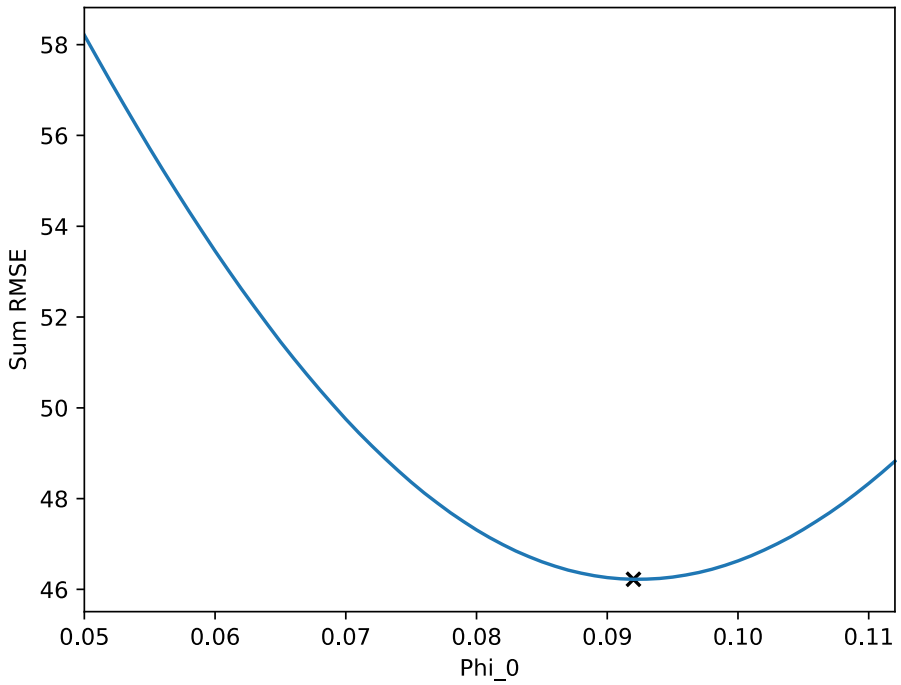


*Figure 2: Effect of varying $\varphi_0(C_3)$ on the summed daily RMSE between flux-derived and modelled GPP at the 17 calibration sites.*

$\phi_0(C_4)$ was not calibrated because $C_4$-dominated vegetation was not represented among the calibration set of sites. Skillman (2008) gives a typical value of $\phi_0 = 0.058$ for $C_4$ plants and we propose that this value be used.

Figure 3 shows the results of data-model comparison in the form of time series of GPP from the flux measurements, and from the P model with optimized $\phi_0(C_3)$ according to the updated calibration. (Note that this Figure is reproduced in full here; the coloured model traces were inadvertently omitted from the published v2.1.) Visual agreement and RMSE values proved generally satisfactory. There were some mismatches, which do not appear to be related to vegetation type. GPP was generally underestimated at AU-Tum, for unknown reasons. Mismatches include underestimation of peak-season GPP by the model at a few sites; and in some sites and years, the simulation of positive GPP around the start and/or end of the growing season at times when the flux-derived GPP is close to zero. This latter problem was alleviated, although not completely removed, by the substition of LST for air temperature as a driver. Peaks in observed GPP during winter, e.g. at CA-NS3, were not simulated but are presumed to be artefacts.

Figure 4 shows modelled GPP, with uncertainties, as provided for validation, in two versions: one driven by ECMWF temperature data, the other driven by LST data. Figure 5 illustrates the effects of including SWI as a modifier of GPP in the model driven by ECMWF temperature data. It can be seen that the effect of including SWI is closely similar to the effect of switching from ECMWF temperature to LST, in the two years for which both SWI and LST data were available. This finding suggests that the use of LST has been effective in representing the consequences of soil moisture variations for GPP.

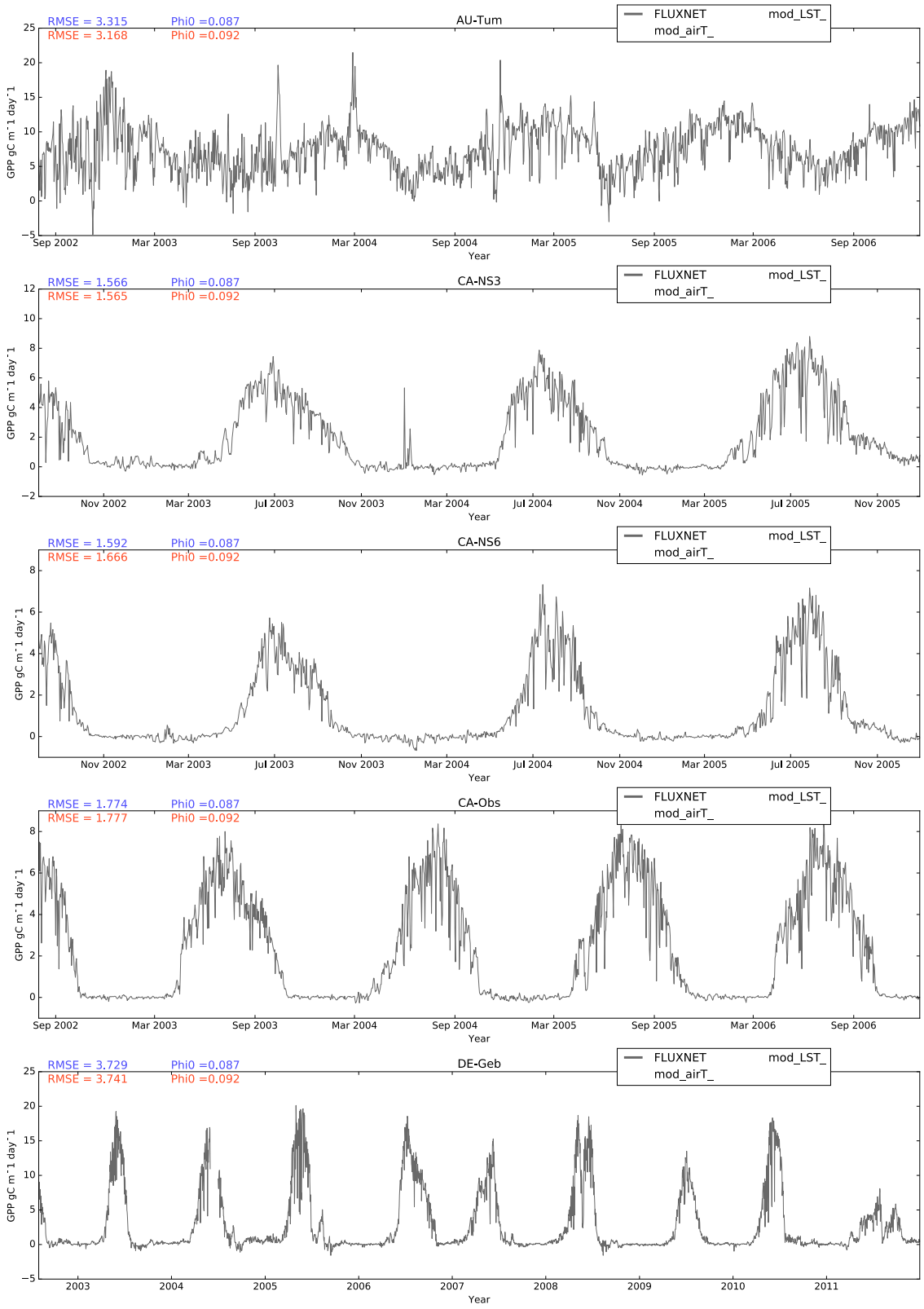
AU-Tum
RMSE = 3.315 Phi0 =0.087
RMSE = 3.168 Phi0 =0.092
FLUXNET mod_LST_
mod_airT_
GPP gC m^-1 day^-1
Year
CA-NS3
RMSE = 1.566 Phi0 =0.087
RMSE = 1.565 Phi0 =0.092
CA-NS6
RMSE = 1.592 Phi0 =0.087
RMSE = 1.666 Phi0 =0.092
CA-Obs
RMSE = 1.774 Phi0 =0.087
RMSE = 1.777 Phi0 =0.092
DE-Geb
RMSE = 3.729 Phi0 =0.087
RMSE = 3.741 Phi0 =0.092

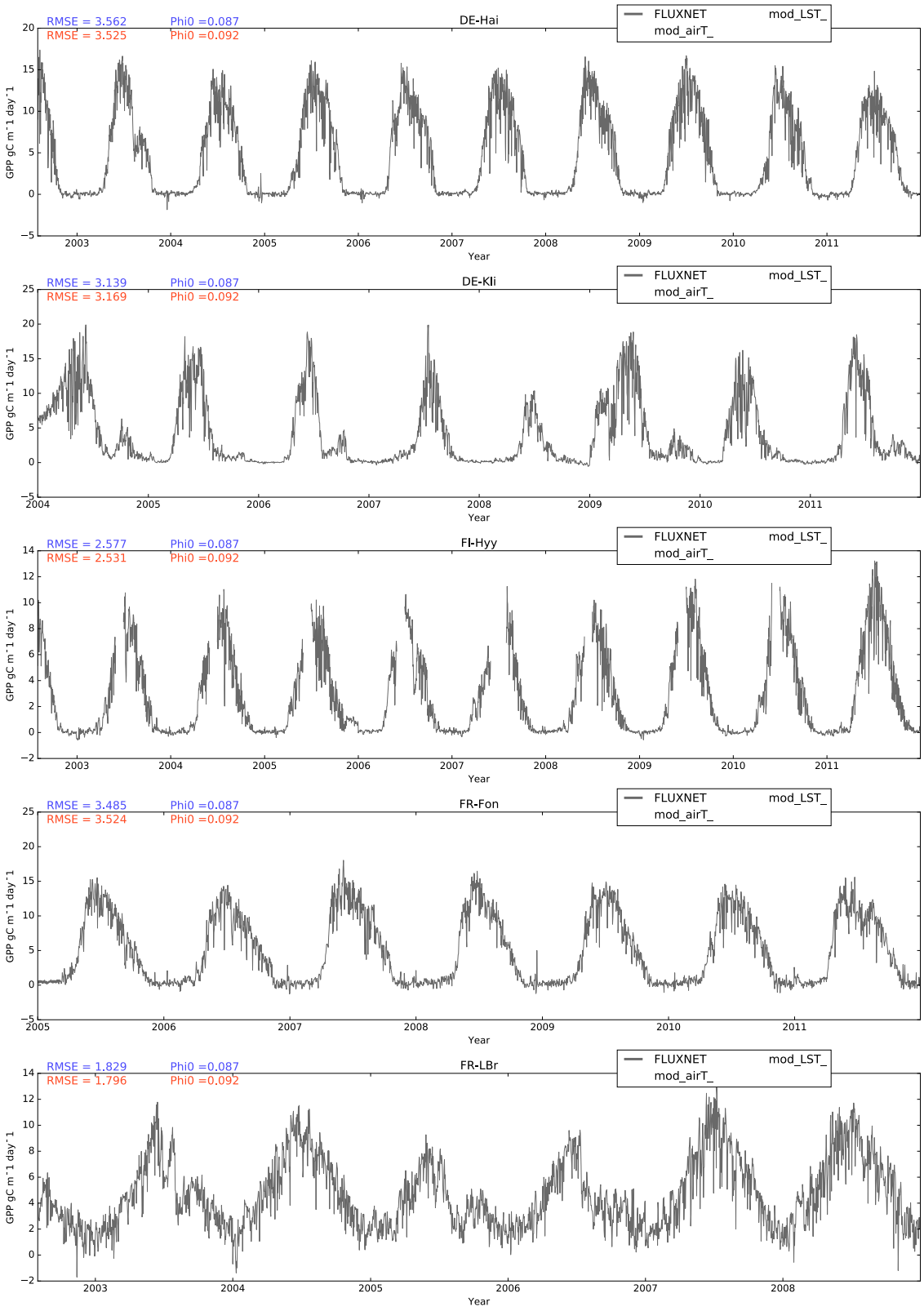
RMSE = 3.562
Phi0 =0.087
RMSE = 3.525
Phi0 =0.092
DE-Hai
FLUXNET
mod_LST_
mod_airT_
GPP gC m^-1 day^-1
Year
RMSE = 3.139
Phi0 =0.087
RMSE = 3.169
Phi0 =0.092
DE-Kli
RMSE = 2.577
Phi0 =0.087
RMSE = 2.531
Phi0 =0.092
FI-Hyy
RMSE = 3.485
Phi0 =0.087
RMSE = 3.524
Phi0 =0.092
FR-Fon
RMSE = 1.829
Phi0 =0.087
RMSE = 1.796
Phi0 =0.092
FR-LBr

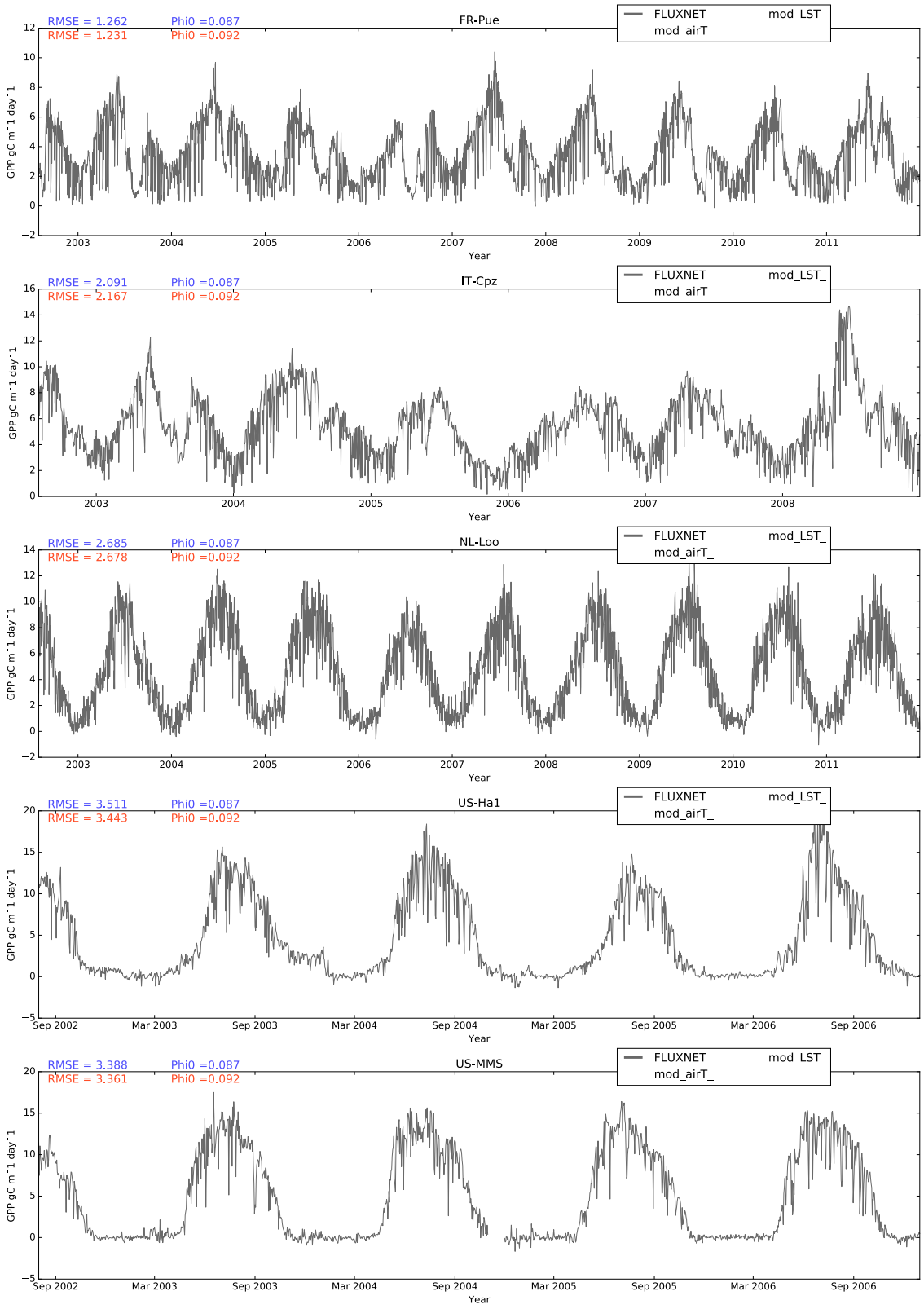
RMSE = 1.262
Phi0 =0.087
RMSE = 1.231
Phi0 =0.092
FR-Pue
FLUXNET
mod_LST_
mod_airT_
GPP gC m^-1 day^-1
Year
RMSE = 2.091
Phi0 =0.087
RMSE = 2.167
Phi0 =0.092
IT-Cpz
RMSE = 2.685
Phi0 =0.087
RMSE = 2.678
Phi0 =0.092
NL-Loo
RMSE = 3.511
Phi0 =0.087
RMSE = 3.443
Phi0 =0.092
US-Ha1
Sep 2002
Mar 2003
Sep 2003
Mar 2004
Sep 2004
Mar 2005
Sep 2005
Mar 2006
Sep 2006
RMSE = 3.388
Phi0 =0.087
RMSE = 3.361
Phi0 =0.092
US-MMS

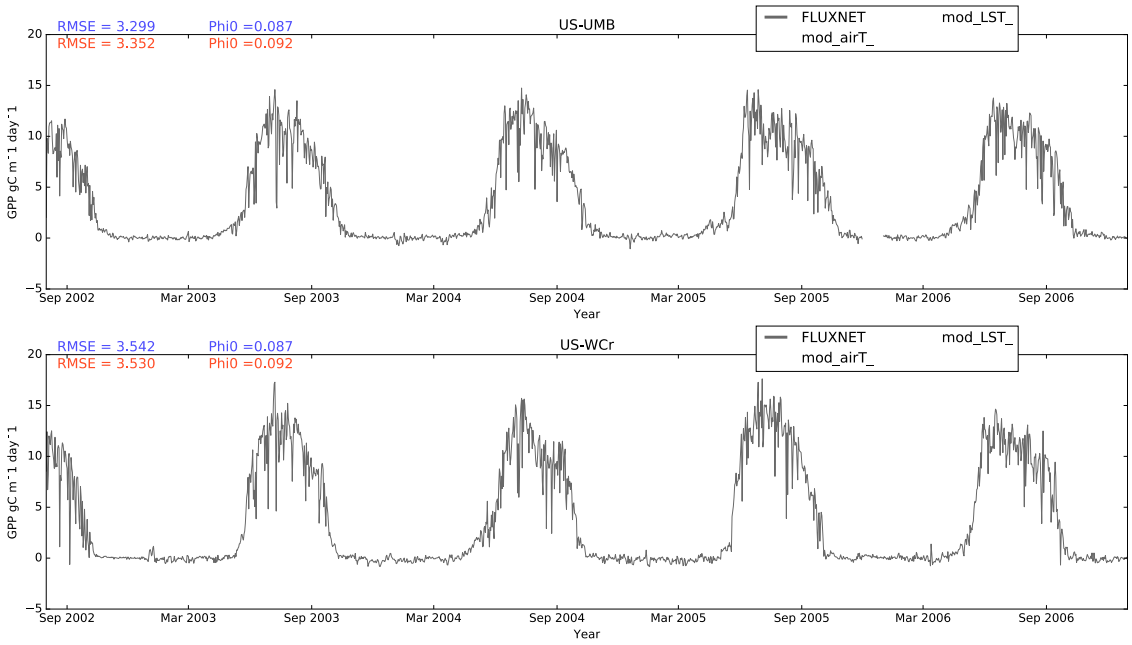


*Figure 3: Comparison of flux-derived GPP and P model-simulated GPP at the calibration sites. The dark grey traces represent the mean GPP from the alternative FLUXNET partitioning methods. The red traces represent modelled GPP (updated calibration driven by LST); the blue traces represent modelled GPP driven by air temperature.*

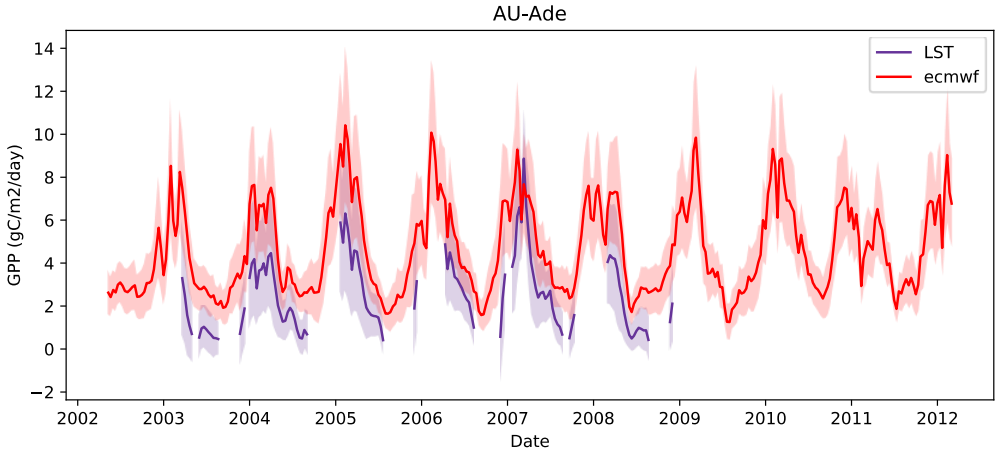

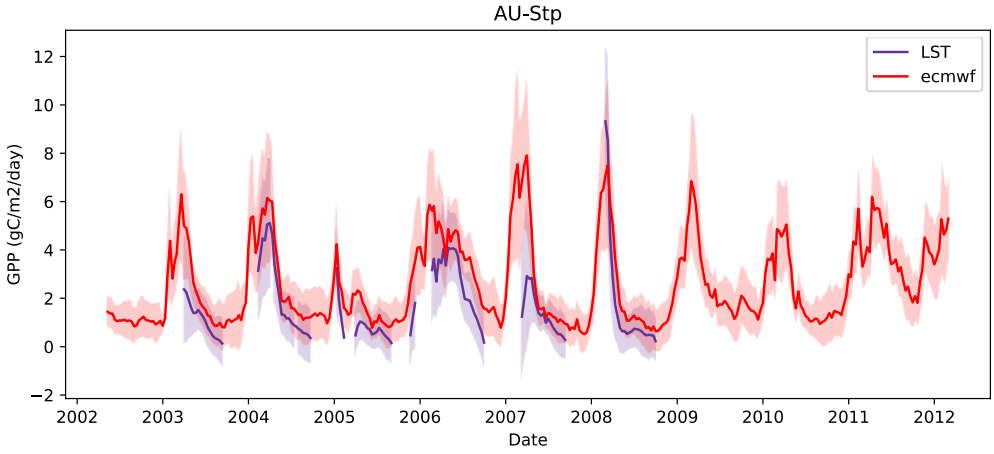
AU-Stp
LST
ecmwf
GPP (gC/m2/day)
Date

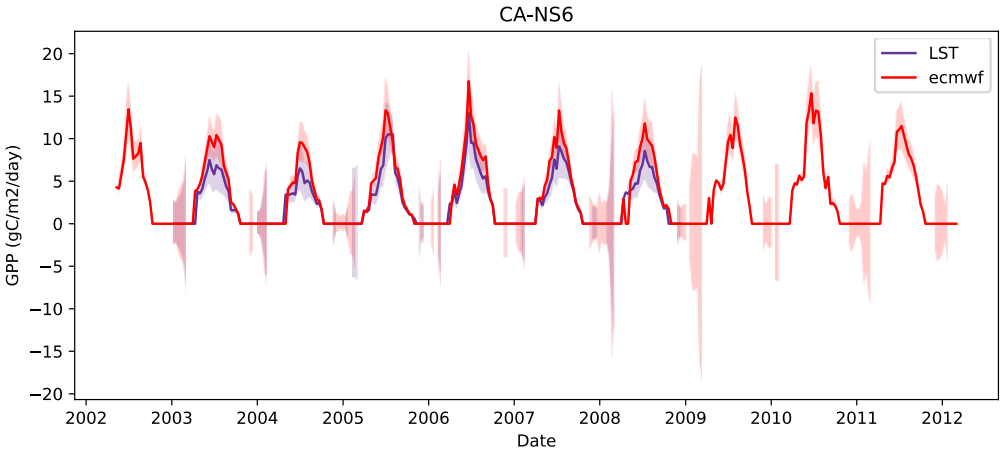
CA-NS6
LST
ecmwf
GPP (gC/m2/day)
Date

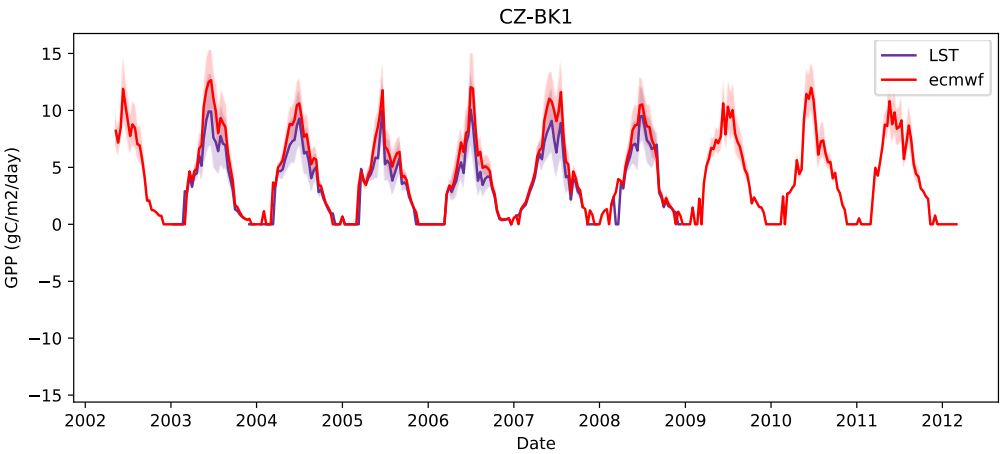
CZ-BK1
LST
ecmwf
GPP (gC/m2/day)
Date

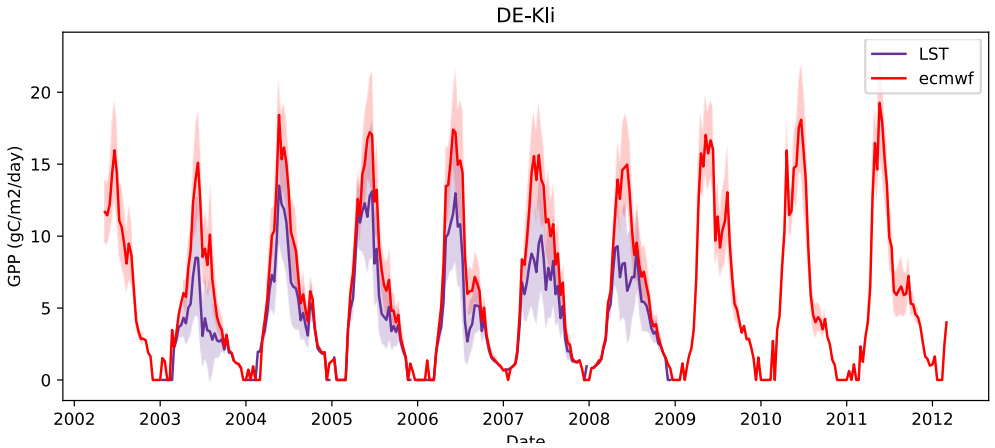
DE-Kli
LST
ecmwf
GPP (gC/m2/day)
0
5
10
15
20
2002
2003
2004
2005
2006
2007
2008
2009
2010
2011
2012
Date

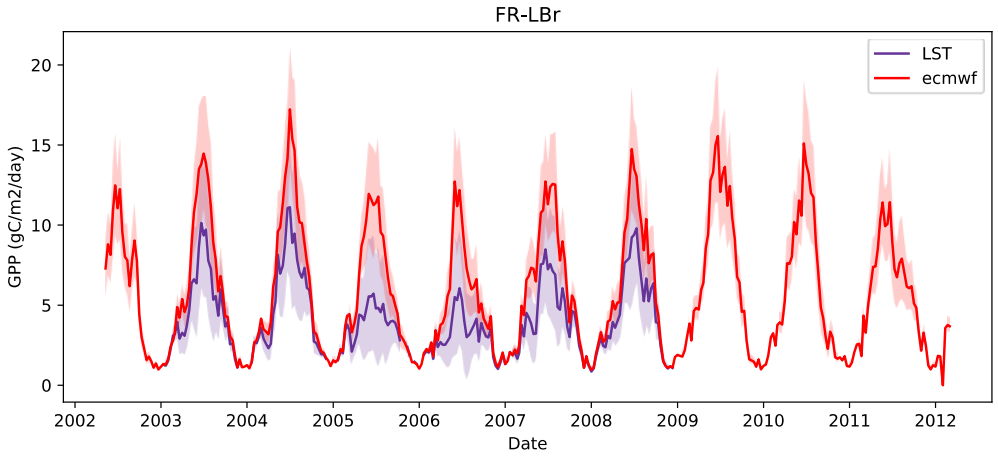
FR-LBr
LST
ecmwf
GPP (gC/m2/day)
0
5
10
15
20
2002
2003
2004
2005
2006
2007
2008
2009
2010
2011
2012
Date

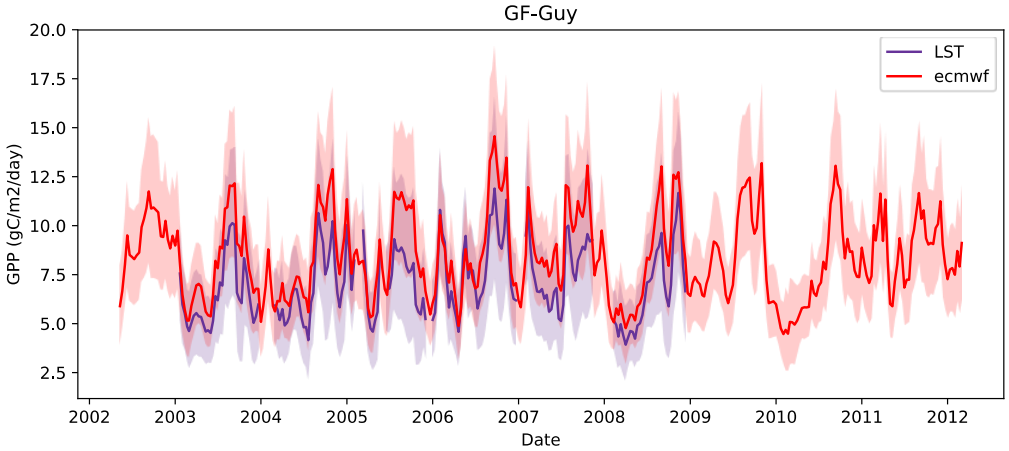
GF-Guy
LST
ecmwf
GPP (gC/m2/day)
2.5
5.0
7.5
10.0
12.5
15.0
17.5
20.0
2002
2003
2004
2005
2006
2007
2008
2009
2010
2011
2012
Date

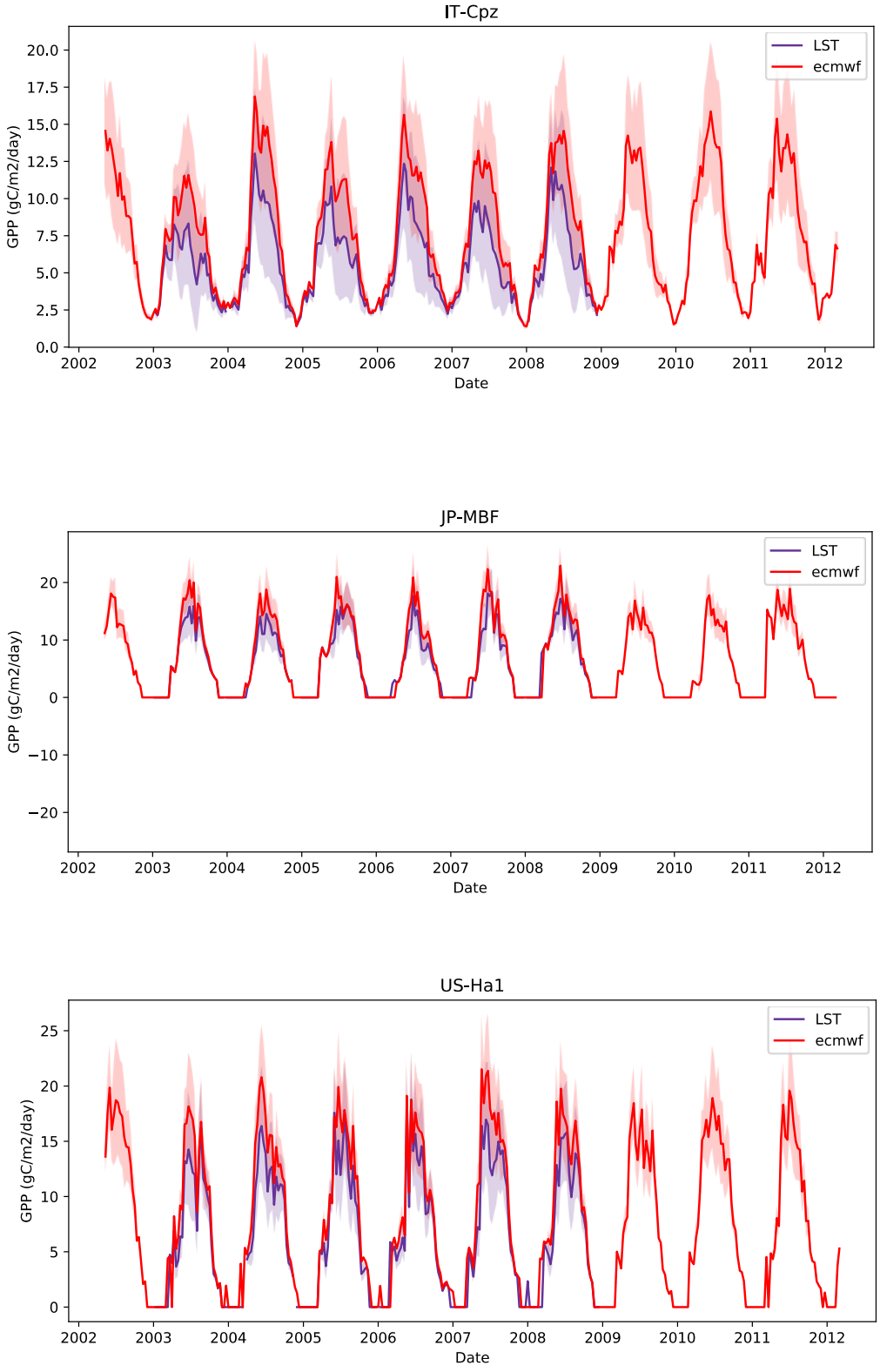


*Figure 4: Examples of P model-simulated GPP outputs (with uncertainties) as provided for the validation, with temperature either interpolated from ECMWF meteorological data, or derived from remotely sensed LST.*

*Figure 5: Examples of alternative P model simulations of GPP at two flux sites. The dark grey traces represent the range of GPP obtained from the alternative FLUXNET partitioning methods. Blue: temperatures from ECMWF. Red: temperatures from LST. Green: temperatures from ECMWF, GPP modified by Copernicus SWI according to Stocker et al. (2018b).*

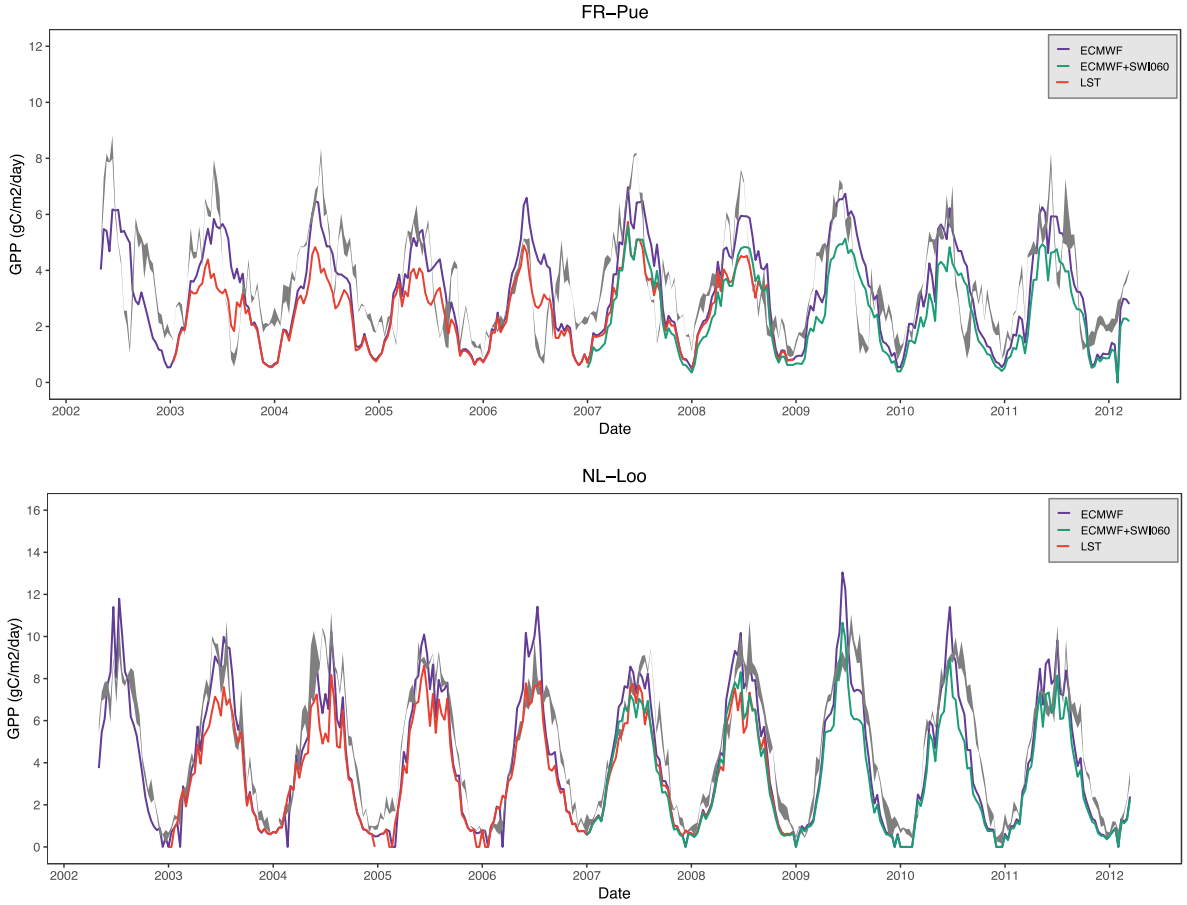


## 4.6. DERIVATION OF ABOVE-GROUND PRODUCTION EFFICIENCY FUNCTIONS

A meta-analysis of the controls of ABPE was based on 117 unique sites represented in four data sets: an unpublished literature review by Alessio Collalti, Euro-Mediterranean Center on Climate Change, Italy; the Forests data set (Luyssaert et al., 2007) with supplementary data provided by Sara Vicca, University of Antwerp; the Grasslands and Croplands dataset, also provided by Sara Vicca; and the ForC data set (Anderson-Texeira et al., 2018). The selection criteria for sites were (a) the availability of *independent* measures of both ABP and GPP, (b) information on management (and stage age in the case of forests), and (c) geographic coordinates. Mean annual temperature (MAT, °C) and annual precipitation total (Ppn, mm) data were derived from the data set if provided, or otherwise estimated using the CHELSA data (Karger *et al.*, 2017). Forest sites were classified as fertilized and/or irrigated (FI), otherwise managed (M), unmanaged or pristine (UM), and recently disturbed (RD). Forest stand age was log-transformed to alleviate skewness. The age of old-growth forests was arbitrarily set to 999 years.

Data exploration and initial regressions highlighted four potential outliers, which were excluded from subsequent analyses: two sites with ABPE > 0.9 (one forest site and one maize crop), and two forest sites that generated very high residual values in an initial analysis with ABPE 0.09 and 0.70 respectively. Model selection followed a protocol recommended by Zuur et al. (2009). An ordinary least-squares multiple linear regression model was compared with a mixed-effects model that shared the same fixed terms, but included a random intercept term for sites. The mixed-effects model was not preferred on either log-likelihood or Akaike information criteria, so simpler fixed-effects models were adopted throughout.

#### 4.6.1. FORESTS AND PLANTATIONS

Commencing with a "beyond optimal" model (management + log(age) + MAT + Ppn), backward stepwise selection yielded a final model that predicts ABPE in forests as a function of management, age and Ppn (Model 2 in Table 4; $R^2$ = 0.35). Bioclimatic indices (CHELSA) for mean temperature of the warmest quarter and the seasonality of temperature and rainfall were also included in model iterations, but offered no improvement in explanatory power. Model residuals (Model 2, Table 4) were well behaved and gave no concern for the underlying assumptions of equality of variance and normality. There was no discernible pattern in plots of model residuals against MAT, supporting the decision to exclude MAT from the final model.

*Table 4 Selection steps for multiple regression models to predict ABPE.*

| Model | Explanatory variables | Step | df | AIC | RSS |
|---|---|---|---|---|---|
| 1 | Mgmt_code + log(age) + MAT + Ppn | | 8 | -357.51 | 0.717 |
| 2 | Mgmt_code + log(age) + Ppn | *drop MAT* | 7 | -359.46 | 0.717 |
| 3 | Mgmt_code + log(age) + MAT | *drop Ppn* | 7 | -352.38 | 0.784 |
| 4 | Mgmt_code + MAT + Ppn | *drop age* | 7 | -352.09 | 0.787 |
| 5 | log(age) + MAT + Ppn | *drop Mgmt* | 5 | -348.75 | 0.864 |

The analysis indicated that ABPE is lowest in unmanaged forest sites with low rainfall, and that efficiency declines with stand age (Figure 6). Excluding old-growth forest sites left this model virtually unchanged.

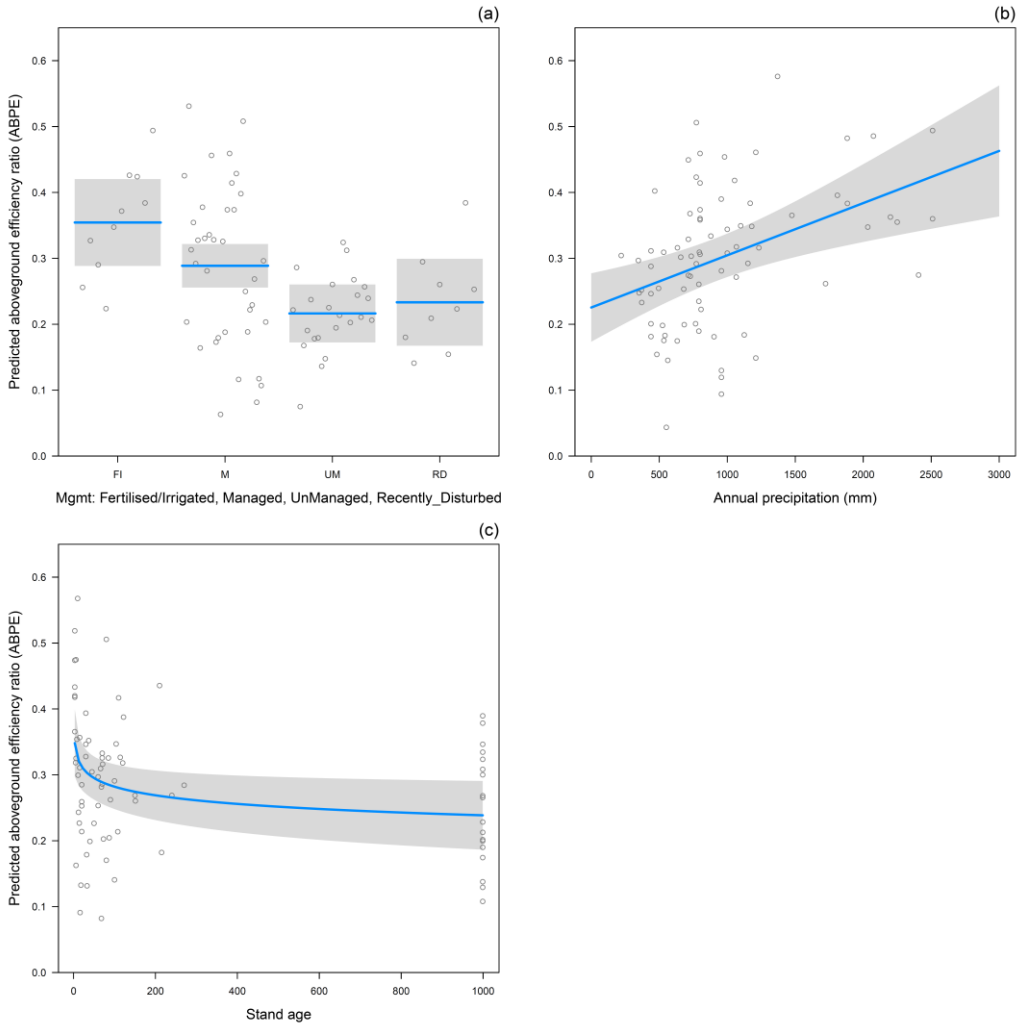


*Figure 6 Forest sites: partial residual plots showing ABPE as a function of management regime, annual precipitation and stand age. The first plot illustrates the effect of management regime while holding precipitation and age at their median values.*

The derived equation for ABPE in forests, illustrated in Figure 6, is as follows:

$$ABPE = i_m - \gamma_{age} \log_{10}(age) + \gamma_{Ppn} Ppn$$

where:

$i_m$ = 0.371 ± 0.043 (fertilized and/or irrigated)
0.306 ± 0.036 (otherwise managed)
0.233 ± 0.039 (unmanaged)
0.250 ± 0.046 (recently disturbed)

$\gamma_{age}$ = 0.043 ± 0.016

$\gamma_{Ppn}$ = 0.079 ± 0.022 x $10^{-3}$ $mm^{-1}$

### 4.6.2. GRASSLAND AND CROPLANDS

Fewer data were available for non-forest systems ($n$ = 29), especially for crops, where the chief difficulty was in finding studies that provided independent estimates of ANPP and GPP. Statistical power was limited. The selection steps arrived at a linear model that predicted ABPE simply as a function of ecosystem (grass or crop; $R^2$ = 0.53). Model variants that included management regime as an additional explanatory term suffered from the absence of a fully crossed Ecosystem: Management design. Such addiditive models were not preferred on log-likelihood or Akaike criteria even when management regime was simplified to two categories, 'managed' versus 'unmanaged'. None of the available environmental variables or indices added to explanatory power for these non-forest sites.

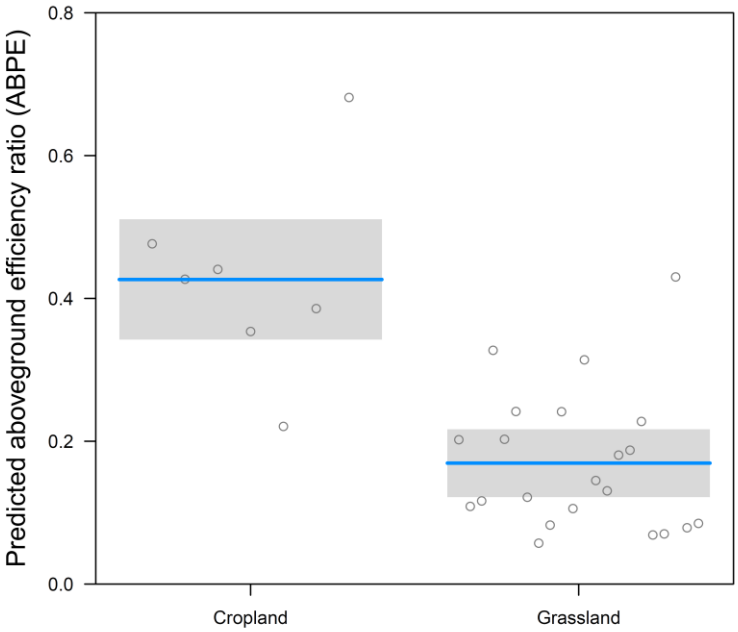


*Figure 7 Non-forest sites: Partial residual plots showing ABPE as a function of ecosystem type.*

Croplands show substantially higher ABPE than grasslands (Figure 7). Given the small sample sizes in this analysis, the following generic values of ABPE are proposed: 0.43 ± 0.04 for crops and 0.17 ± 0.05 for grasslands.

# CHAPTER 5 VALIDATION APPROACH

This chapter summarizes the validation and proposed comparative benchmarking of the products:

(1) Point-location time series of modelled GPP (as illustrated in Figure 4 above) have been compared with *in situ* flux measurements of GPP to assess their accuracy, and to compare the performance of the LST and ECMWF versions, as documented in the Validation Report. Modelled GPP has also been provided for the set of ABP validation sites. Validation will involve applying the appropriate ABPE functions for each site.

(2) The global spatial GPP/ABP products are being compared to other operational EO products (MODIS, C-GLOPS1) to assess how much, and where, the new products differ from existing ones.

## 5.1. VALIDATION METHOD AGAINST IN-SITU DATA

Validation aims to assess the capability of model simulations to describe carbon dynamics for a variety of ecosystems and to identify potential ways to improve them. A separate Validation Report tests how well the GPP simulations describe annual carbon dynamics for different ecosystems and climates; encompass the daily and seasonal trends of GPP; describe interannual variability; and describe the main environmental controls of GPP.

### 5.1.1. DESCRIPTION OF THE IN SITU DATA

Validation of modelled GPP relies on the FLUXNET 2015 database of values obtained with the eddy-covariance technique. This well-established technique provides GPP by post-processing of direct measurements of net ecosystem $CO_2$ exchange. FLUXNET includes data from regional networks, international projects and field-sites of research institutes and provides a thoroughly standardized data treatment and data analysis for sites distributed across the world. These data have been extensively used for the development and evaluation of ecological models at regional or global scale.

The FLUXNET GPP data are well suited to use as validation products for several reasons: (i) they are available at both high time resolution (half-hourly) and aggregated to longer time steps (daily to annual); (ii) they are available for multiple years (>10 years for the most intensively studied sites); (iii) they typically measure an area of the ecosystem (footprint) comparable to the resolution of remote sensed products; (iv) data are provided with uncertainty estimations; and (v) sites are available globally and for all types of terrestrial ecosystems, including forests, savannas, grasslands, croplands, wetlands and tundra. FLUXNET was established in 1998 (Baldocchi et al., 2001) and since then techniques have improved and different database versions have been produced. We use the latest version (FLUXNET 2015) and confine attention to publicly available data, for which data use is free and open provided that proper acknowledgment is given to site PIs and funding agencies (Tier 1, see http://fluxnet.fluxdata.org/data/fluxnet2015-dataset/). About 200-250 GPP sites are publicly available now, of which 122 met our criteria for quality, homogeneity and length of record.

ABP validation is being carried out using a large ABP dataset assembled by the University of Antwerp group.

#### 5.1.2. VALIDATION METHOD

Validation is being carried out at high spatial resolution i.e. at site level; we do not plan to perform landscape or regional validations, as this would require up-scaling of *in situ* data with a large propagation of uncertainty. A new fAPAR data set was applied. Otherwise, the model and its data inputs follow the same protocol as was used for the updated calibration and presented in Figures 2 and 3 above. These outputs also include uncertainties (by site and dekad) in modelled GPP calculated by the method described above. Some examples of these outputs, representing major biomes, are illustrated in Figure 4.

### 5.2. BENCHMARK METHOD TO OTHER DATA SETS

#### 5.2.1. REFERENCE DATA SETS

At global scale a comparison with two operational EO GPP/NPP products, both discussed in Chapter 3 above, is underway:

**The C-GLOPS1 Dry Matter Production (DMP) product** at 10-daily time steps and expressed in kg DM $ha^{-1}$ $day^{-1}$. The DMP is generated by a LUE model first implemented by Veroustraete (1994) and modified and improved in the MARSOP and Copernicus Global Land Service project to run on SPOT-VGT/PROBA-V imagery and ECMWF meteorological data. Within C-GLOPS, the product has been extensively validated against in-situ, MODIS and other modelled datasets of GPP and NPP. The ATBD and validation report of the DMP are available through the C-GLOPS website, http://land.copernicus.eu. The current online version 1 is based on 1 km SPOT-VGT and PROBA-V fAPAR data derived from the MARSOP project. In the meantime, a second version of the DMP is in development and has been validated. Besides a number of algorithmic changes, this version is based on an improved dataset of SPOT-VGT and PROBA-V fAPAR. Both products are being compared with the P-model output.

**MODIS GPP (MOD17A2) and NPP (MOD17A3)** as described in detail by Running et al. (1999), Heinsch et al. (2003) and Zhao et al. (2005). This is also a variant of the satellite-based LUE approach. The GPP product is available at 8-daily timesteps. The NPP product is derived on an annual basis using maintenance and growth respiration estimates linking daily biomass and annual growth of plant tissues to the satellite-derived estimates of leaf area index (LAI). The MYD17A3H Version 6 product, recently released by MODIS, provides estimated annual NPP at 500 m pixel resolution. Annual NPP is derived from the sum of the 45 8-day Net Photosynthesis (PSN) products (MYD17A2H) from the given year.

#### 5.2.2. METHODS

The methods for the benchmarking of the different EO-derived vegetation production data sets are based on guidelines, protocols and metrics defined by the Land Product Validation (LPV) group of the Committee on Earth Observation Satellite (CEOS) for the validation of satellite-derived land products. The following aspects will be evaluated.

(1) *Product completeness*: the missing values or pixels flagged as invalid over land were quantified, overall and over different biomes. An aggregated version of the ESA CCI land cover map will used for this purpose.
(2) Spatial consistency analysis:

- *Spatial distribution of the GPP/NPP values*: global maps of metrics expressing the similarity and difference between different global GPP/NPP time series will be computed. The metrics include the Root Mean Squared Error (RMSE).
- *Magnitude of the retrievals*: global yearly averages will be calculated for GPP and NPP.

(3) Global statistical analysis:

- *Histograms of bias*: histograms of residuals between products.
- *Distribution per biome type*: statistical distributions of GPP/NPP values and residuals, computed over biomes for the different data sets. An aggregated version of the ESA CCI land cover map will used for this purpose.
- *Global statistics*: Scatterplots between the different datasets will be produced at a global scale and per biome. Metrics (e.g. coefficient of determination, agreement coefficient, orthogonal regression) among different data sets are computed per biome.

(4) Temporal consistency analysis

- *Temporal variation*: Statistical metrics among different data sets are computed per scene to evaluate the time evolution of the metrics.

## REFERENCES


Ainsworth, E.A. and S.P. Long (2005) What have we learned from 15 years of free-air $CO_2$ enrichment? A meta-analytic review of the responses of photosynthesis, canopy properties and plant production to rising $CO_2$. *New Phytologist* **165**: 351–372.

Allen, R.G., L.S. Pereira, D. Raes and M. Smith (1999) Crop evapotranspiration – Guidelines for computing crop water requirements. *FAO Irrigation and Drainage Paper* **56.**

Anav, A., P. Friedlingstein, C. Beer, P. Ciais, A. Harper, C. Jones, G. Murray-Tortarolo, D. Papale, N.C. Parazoo and P. Peylin (2015) Spatiotemporal patterns of terrestrial gross primary production: a review. *Reviews of Geophysics* **53**: 785–818.

Anderson-Teixeira, K.J., M.M.H. Wang, J.C. McGarvey, V. Herrmann, A.J. Tepley, B. Bond-Lamberty and D.S. LeBauer (2018) ForC: a global database of forest carbon stocks and fluxes. *Ecology* **99**: 1507–1507.

Atkin, O.K., K.J. Bloomfield, P.B. Reich, M.G. Tjoelker, G.P. Asner, D. Bonal, G. Bönisch, M. Bradford, L.A. Cernusak, E.G. Cosio, D. Creek, K.Y. Crous, T. Domingues, J.S. Dukes, J.J.G. Egerton, J.R. Evans, G.D. Farquhar, N.M. Fyllas, P.P.G. Gauthirt, E. Gloor, T.E. Gimeno, K.L. Griffin, R. Guerrieri, M.A. Heskel, C. Huntingford, F.Y. Ishida, J. Kattge, H. Lambers, M.J. Liddell, J. Lloyd, C.H. Lusk, R.E. Martin, A.P. Maksimov, T.C. Maximov, Y. Malhi, B.E. Medlyn, P. Meir, L.M. Mercado, N. Mirotchnik, D. Ng, Ü. Niinemets, O.S. O'Sullivan, O.L. Philips, L. Poorter, P. Poot, I.C. Prentice, N. Salinas, L.M. Rowland, M.G. Ryan, S. Sitch, M. Slot, N.G. Smith, M.H. Turnbull, M.C. VanderWel, F. Valladares, E.J. Veneklaas, L.K. Weerasinghe, C. Wirth, I.J. Wright, K. Wythers, J. Xiang, S. Xiang and J. Zaragoza-Castells (2015) Global variability in leaf respiration in relation to climate, plant functional types and leaf traits. *New Phytologist* **206**: 614–636.

Bernacchi, C.J., E.L. Singsaas, C. Pimentel, A.R. Portis Jr and S.P. Long (2001) Improved temperature response functions for models of Rubisco-limited photosynthesis. *Plant, Cell and Environment* **24**: 253–259.

Campiolo, M. S. Vicca, S. Luyssaert, J. Bilcke, E. Ceschia, F.S. Chapin III, P. Ciais, M. Fernández-Martínez, Y. Malhi, M. Obersteiner, D. Olefeldt, D. Papale, S.L. Piao, J. Peñuelas, P.F. Sullivan, X. Wang, T. Zenonen and I.A. Janssens (2015) Biomass production efficiency controlled by management in temperate and boreal ecosystems. *Nature Geoscience* **8**: 843–846.

Ceballos, A., K. Scipal, W. Wagner and J. Martínez-Fernández (2005) Validation of ERS scatterometer-derived soil moisture data in the central part of the Duero Basin, Spain. *Hydrological Processes* **19**: 1549-1566.

Ceccherini, G., N. Gobron, N and M. Robustelli (2013) Harmonization of Fraction of Absorbed Photosynthetically Active Radiation (FAPAR) from Sea-Viewing Wide Field-of-View Sensor (SeaWiFS) and Medium Resolution Imaging Spectrometer Instrument (MERIS). *Remote Sensing* **5**: 3357-3376.

De Kauwe, M.G., T.F. Keenan, B.E. Medlyn, I.C. Prentice and C. Terrer (2016a) Satellite based estimates underestimate the effect of $CO_2$ fertilization on NPP. *Nature Climate Change* **6**: 892–893.

De Kauwe, M.G., Y.-S. Lin, I.J. Wright, B.E. Medlyn, K.Y. Crous, D.S. Ellsworth, V. Maire, I.C. Prentice, O.K. Atkin, A. Rogers, Ü. Niinemets, S. Serbin, P. Meir, J. Uddling, H.F. Togashi, L. Tarvainen, L.K. Weerasinghe, B.J. Evans, F.Y. Ishida and T. F. Domingues (2016b) A test of a "one-point method" for estimating maximum carboxylation capacity. *New Phytologist* **210**: 1130–1144.

Dee, D.P., S.M. Uppala, A.J. Simmons, P. Berrisford, P. Poli, S. Kobayashi, U. Andrae, M.A. Balmaseda, G. Balsamo, P. Bauer, P. Bechtold, A.C.M. Beljaars, L. van der Berg, J. Bidlot, N. Bormann, C. Delsol, R. Dragani, M. Fuentes, A.J. Geer, L. Haimberger, S.B. Healy, H. Hersbach, E.V. Hólm, L. Isaksen, P. Kållberg, M. Köhler, M. Matricardi, A.P. McNally, B.M. Monge-Sanz, J.-J. Morcrette, B.-K. Park, C. Peubey, P. de Rosnay, C Tavolato, J.-N. Thépaut and F. Vitart (2011) The ERA-Interim reanalysis: configuration and performance of the data assimilation system. *Quarterly Journal of the Royal Meteorological Society* **137**: 553–597.

Dewar, R.C. (1996) The correlation between plant growth and intercepted radiation: an interpretation in terms of optimal plant nitrogen content. *Annals of Botany* **78**: 125–136.

Donohue, R.J., I.H. Hume, M.L. Roderick, T.R. McVicar, J. Beringer, L.B. Hutley, J.C. Gallant, J.M. Austin, E. can Gorsel, J.R. Cleverly, W.S. Meyer and S.K. Arndt (2014) Evaluation of the remote-sensing-based DIFFUSE model for estimating photosynthesis of vegetation. *Remote Sensing of Environment* **155**: 349–365.

Donohue, R.J., M.L. Roderick, T.R. McVicar and G.D. Farquhar (2013) Impact of $CO_2$ fertilization on maximum foliage cover across the globe's warm, arid environments. *Geophysical Research Letters* **40**: 1–5.

Farquhar, G.D., S. von Caemmerer and J. Berry (1980) A biochemical model of photosynthetic $CO_2$ assimilation in leaves of $C_3$ species. *Planta* **149**: 78–90.

Fernández-Martínez, M., S. Vicca, I.A. Janssens, P. Ciais, M. Obersteiner, M. Bartrons, J. Sardans, A. Verger, J.G. Canadell, F. Chevallier, X. Wang, C. Bernhoffer, P.S. Curtis, D. Gianelle, T. Grünwald, B. Heinesch, A. Ibrom, A. Knohl, T. Laurila, B.E. Law, J.M. Limousin, B. Longdoz, D. Loustau, I. Mammarella, G. Matteucci, R.K. Monson, L. Montagnani, E.J. Moors, J.W. Munger, D. Papale, S.L. Piao and J. Peñuelas (2017) Atmospheric deposition, $CO_2$, and change in the land carbon sink. *Scientific Reports* **7**: 9632.

Garbulsky, M.F., J. Peñuelas, D. Papale, J. Ardö, M.L. Goulden, G. Kiely, A.D. Richardson, E. Rotenberg, E.M. Veenendaal and I. Filella (2010) Patterns and controls of the variability of radiation use efficiency and primary productivity across terrestrial ecosystems. *Global Ecology and Biogeography* **19**: 253–267.

Gill, A.L. and A.C. Finzi (2016) Belowground carbon flux links biogeochemical cycles and resource-use efficiency at the global scale. *Ecology Letters* **19**: 1419–1428.

Ghent, D. (2012) *Land Surface Temperature Validation and Algorithm Verification*. Report to European Space Agency (UL-NILU-ESA-LSTVAV).

Goetz, S.J., S.D. Prince, S.N. Goward, M.M. Thawley and J. Small (1999) Satellite remote sensing of primary production: an improved production efficiency modeling approach. *Ecological Modelling* **122**: 239–255.

Graven, H.D., R.F. Keeling, S.C. Piper, P.K. Patra, B.B. Stephens, S.C. Wofsy, L.R. Welp, C. Sweeney, P.P. Tans, J.J. Kelley, B.C. Daube, E.A. Kort, G.W. Santoni and J.D. Bent (2013) Enhanced seasonal exchange of $CO_2$ by northern ecosystems since 1960. *Science* **341**: 1085–1089.

Haxeltine, A. and I.C. Prentice (1996) A general model for the light use efficiency of primary production. *Functional Ecology* **10**: 551–561.

Hermida-Carrera, C., M.V. Kapralov and J. Galmés (2016) Rubisco catalytic properties and temperature response in crops. *Plant Physiology* **171**: 2549–2561.

Karger, D.N., O. Conrad, J. Bohner, T. Kawohl, H. Kreft, R.W. Soria-Auza, N.E. Zimmermann, H.P. Linder and M. Kessler (2017) Data Descriptor: Climatologies at high resolution for the earth's land surface areas. *Scientific Data* **4**.

Kattge, J. and W. Knorr (2007) Temperature acclimation in a biochemical model of photosynthesis: a reanalysis of data from 36 species. *Plant Cell and Environment* **30:** 1176–1190.

Keeling, C.D., S.C. Piper, R.B. Bavastow, M. Wahlen, T.P. Whorf, M.R. Raupach and H.A. Meijer (2001) Exchanges of atmospheric $CO_2$ and $^{13}CO_2$ with the terrestrial biosphere and oceans from 1978 to 2000. I. Global aspects. *SIO Reference Series* **01–06**, Scripps Institution of Oceanography, 88 pp.

Keenan, T.F., I.C. Prentice, J.G. Canadell, C. Williams, H. Wang, M.R. Raupach and G.J. Collatz (2016) Recent pause in the growth rate of atmospheric $CO_2$ due to enhanced terrestrial uptake. *Nature Communications* **7**: 13428.

Knorr, W. and M. Heimann (1995) Impact of drought stress and other factors on seasonal land biosphere $CO_2$ exchange studied through an atmospheric tracer transport model. *Tellus B* **47**: 471–489.

Landsberg, J.J. and R.H. Waring (1997) A generalised model of forest productivity using simplified concepts of radiation-use efficiency, carbon balance and partitioning. *Forest Ecology and Management* **95**: 209–228.

Lin, X., B. Chen, J. Chen, H. Zhang, S. Sun, G. Xu, L. Guo, M. Ge, J. Qu, L. Li and Y. Kong (2017) Seasonal fluctuations of photosynthetic parameters for light use efficiency models and the impacts on gross primary production estimation. *Agricultural and Forest Meteorology* **236**: 22–35.

Lin, Y.-S., B.E. Medlyn, R.A. Duursma, I.C. Prentice, H. Wang, D. Eamus, C.V.M. Barton, J. Bennie, D. Bonal, A. Bosc, M.S.J. Broadmeadow, L.A. Cernusak, P. De Angelis, A.C. Lola da Costa, J.E. Drake, D.S. Ellsworth, M. Freeman, O. Ghannoum, T.E. Gimeno, Q. Han, K. Hikosaka, L.B. Hutley, J.W. Kelly, K. Kikuzawa, P. Kolari, K. Koyama, J.-M. Limousin, M.L. Linderson, M. Löw, C. Macinnis-Ng, N.K. Martin-StPaul, P. Meir, T.N. Mikkelsen, P. Mitchell, J.B. Nippert, T.W. Ocheltree, Y. Onoda, M. Op de Beeck, V. Resco de Dios, A. Rey, A. Rogers, L. Rowland, N. Salinas, S.A. Setterfield, W. Sun, L. Tarvainen, S. Tausz-Posch, D.T. Tissue, J. Uddling, G. Wallin, J.M. Warren, L. Wingate and J. Zaragoza-Castells (2015) Optimal stomatal behaviour around the world: synthesis of a global stomatal conductance database. *Nature Climate Change* **5**: 459–464.

Luyssaert, S., I. Inglima, M. Jung, A.D. Richradson, M. Reichstein, D. Papale, S.L. Piao, E.-D. Schulze, L. Winmgate, G. Matteucci, L. Aragao, M. Aubinet, C. Beer, C. Bernhofer, K.G. Black, D. Bonal, J.-M. Bonnenfond, J. Chambers, P. Ciais, B. Cook, K.J. Davis, A.J. Dolman, B. Gielen, M. Goulden, J. Grace, A. Granier, A. Grelle, T. Griffis, T. Grünwld, G. Guidolotti, P.J. Hanson, R. Harding, D.Y. Hollinger, L.R. Hutyea, P. Kolari, B. Kruijt, W. Kutsch, F. Lagergren, T. Laurila, B.E. Law, G. Le Maire, A. Lindroth, D. Loustau, Y. Malhi, J. Mateus, M. Migliavacca, L. Misson, L. Montagnani, J. Moncrieff, E. Moors, J.W. Munger, E. Nikinmaa, S.V. Ollinger, G. Pita, C. Rebmann, O. Roupsard, N. Saigusa, M.J. Sanz, G. Seufert, C. Sierra, M.-L. Smith, J. Tang, R. Valentini, T. Vesala and I.A. Janssens (2007) $CO_2$ balance of boreal, temperate, and tropical forests derived from a global database. *Global Change Biology* **13**: 2509–2537.

Maire, V., P. Martre, J. Kattge, F. Gastal, G. Esser, S. Fontaine and J.-F. Soussana (2012) The coordination of leaf photosynthesis links C and N fluxes in $C_3$ plant species. *PLOS One* **7**: e38345.

McCallum, I., O. Franklin, E. Moltchanova, L. Merbold, C. Schmullius, A. Shvidenko, D. Schepaschenko and S. Fritz (2013) Improved light and temperature responses for light-use-efficiency-based GPP models. *Biogeosciences* **10**: 6577–6590.

McCallum, I., W. Wagner, C. Schmullius, A. Shvidenko, M. Obersteiner, S. Fritz and S. Nilsson (2009) Satellite-based terrestrial production efficiency modeling. *Carbon Balance and Management* **4**: 8.

Medlyn, B.E. (1998) Physiological basis of the light use efficiency model. *Tree Physiology* **18**: 167–176.

Medlyn, B.E. (2011) Comment on "Drought-Induced Reduction in Global Terrestrial Net Primary Production from 2000 Through 2009". *Science* **333**: 1093.

Medlyn, B.E., R.A. Duursma, D. Eamus, D.S. Ellsworth, I.C. Prentice, C.V.M. Barton, K.Y. Crous, P. De Angelis, M. Freeman and L. Wingate (2011) Reconciling the optimal and empirical approaches to modelling stomatal conductance. *Global Change Biology* **17**: 2134–2144. [Corrigendum: *ibid.* **18**: 3476.]

Meek, D.W., J.L. Hatfield, T.A. Howell, S.B. Idso, S. B. and R.J. Reginato (1984) A generalized relationship between photosynthetically active radiation and solar radiation. *Agronomy Journal* **76**: 939–945.

Monteith, J. (1972) Solar radiation and productivity in tropical ecosystems. *Journal of Applied Ecology* **19**: 747–766.

Monteith, J.L. (1977). Climate and the efficiency of crop production in Britain. *Philosophical Transactions of the Royal Society of London* **281**: 277–294.

Ogutu, B.O. and J. Dash (2013) An algorithm to derive the fraction of photosynthetically active radiation absorbed by photosynthetic elements of the canopy ($FAPAR_{ps}$) from eddy covariance flux tower data. *New Phytologist* **197**: 511–523.

Ogutu, B.O., J. Dash and T.P. Dawson (2013) Developing a diagnostic model for estimating terrestrial vegetation gross primary productivity using the photosynthetic quantum yield and Earth Observation data. *Global Change Biology* **19**: 2878–2892.

Potter, C.S., J.T. Randerson, C.B. Field, P.A. Matson, P.M. Vitousek, H.A. Mooney and S.A. Klooster (1993) Terrestrial ecosystem production: a process model based on global satellite and surface data. *Global Biogeochemical Cycles* **7**: 811–841.

Prentice, I.C. (2013) Ecosystem science for a changing world. *Grantham Institute for Climate Change Discussion Paper* **4**, 16 pp.

Prentice, I.C., N. Dong, S.M. Gleason, V. Maire and I.J. Wright (2014) Balancing the costs of carbon gain and water loss: testing a new quantitative framework for plant functional ecology. *Ecology Letters* **17**: 82–91.

Prentice, I.C., X. Liang, B. Medlyn and Y. Wang (2015) Reliable, robust and realistic: the three R's of next-generation land-surface modelling. *Atmospheric Chemistry and Physics* **15**: 5987–6005.

Prince, S.D. and S.N. Goward (1995) Global primary production: a remote sensing approach. *Journal of Biogeography* **22**: 815–835.

Running, S.W. and E.R. Hunt (1993) Generalization of a forest ecosystem process model for other biomes, BIOME-BGC, and an application for global-scale models. In: J.R. Ehleringer and C.B. Field (eds) *Scaling Physiological Processes: Leaf to Globe*, Academic Press, New York, 141–158.

Running, S., F. Nemani, M. Heinsch, M. Zhao, M. Reeves and H. Hashimoto (2004) A continuous satellite-derived measure of global terrestrial primary production. *BioScience* **54**: 547–560.

Ryu, Y., D.D. Baldocchi, H. Kobayashi, C. van Ingen, J. Li, T.A. Black, J. Beringer, E. van Gorsel, A. Knohl, B.E. Law and O. Roupsard (2011) Integration of MODIS land and atmosphere products with a coupled-process model to estimate gross primary productivity and evapotranspiration from 1 km to global scales. *Global Biogeochemical Cycles* **25**: GB4017.

Samanta, A., M.H. Costa, E.L. Nunes, S.A. Vieira, L. Xu and R.B. Myneni (2011) Comment on "Drought-Induced Reduction in Global Terrestrial Net Primary Production from 2000 Through 2009". *Science* **333**: 1093.

Sitch, S., B. Smith, I.C. Prentice, A. Arneth, A. Bondeau, W. Cramer, J.O. Kaplan, S. Levis, W. Lucht, M.T. Sykes, K. Thonicke, S. Venevsky (2003) Evaluation of ecosystem dynamics, plant geography and terrestrial carbon cycling in the LPJ dynamic global vegetation model. *Global Change Biology* **9**: 161–185.

Skillman, J.B. (2008) Quantum yield variation across the three pathways of photosynthesis: not yet out of the dark. *Journal of Experimental Botany* **59**: 1647–1661.

Smith, N,G., T.F. Keenan, I.C. Prentice, H. Wang, I.J. Wright, Ü. Niinemets, K.Y. Crous, T.F. Domingues, R. Guerrieri, F.Y. Ishida, J. Kattge, E.L. Kruger, V. Maire, A. Rogers, S.P. Serbin, L. Tarvainen, H.F. Togashi, P.A. Townsend, M. Wang, L.K. Weerasinghe and S.-X. Zhou (in press) Global photosynthetic capacity is optimized to the environment. *Ecology Letters*.

Smith, W.K., S.C. Reed, C.C. Cleveland, A.P. Ballantyne, W.R.L. Anderegg, W.R. Wieder, Y.Y. Liu and S.W. Running (2016) Large divergence of satellite and Earth system model estimates of global terrestrial $CO_2$ fertilization. *Nature Climate Change* **6**: 306–310.

Stocker, B.D., F. Joos, R. Roth, R. Spahni, L. Bouwman, S. Zaehle, Xu-Ri and I.C. Prentice (2013) Multiple greenhouse gas feedbacks from the land biosphere under future climate change scenarios. *Nature Climate Change* **3**: 666–672.

Stocker, B.D., J. Zscheischler, T.F. Keenan, I.C. Prentice, J. Peñuelas and S. Seneviratne (2018a) Quantifying soil moisture impacts on light use efficiency across biomes. *New Phytologist* **218**: 1430–1448.

Stocker, B.D., J. Zscheischler, T.F. Keenan, I.C. Prentice, S.I. Seneviratne and J. Peñuelas (2018b) Satellite monitoring underestimates the impact of drought on terrestrial primary production. In review.

Swets, D., B. Reed, J. Rowland and S. Marko (1999) A weighted least-squares approach to temporal NDVI smoothing. In: *Proceedings of the 1999 ASPRS Annual Conference, Portland, Oregon,* pp. 526–536.

Swinnen, E., R. van Hoolst and H. Eerens (2015) *Algorithm Theoretical Basis Document: Dry Matter Productivity (DMP)*. Copernicus, 37 pp.

Tagesson, T., J. Ardö, B. Cappelaere, L. Kergoat, A. Abdi, S. Horion and R. Fensholt (2017) Modelling spatial and temporal dynamics of gross primary production in the Sahel from earth-observation-based photosynthetic capacity and quantum efficiency. *Biogeosciences* **14**: 1333–1348.

Tang, X., H. Li, N. Huang, X. Li, X. Xu, Z. Ding and J. Xie (2015) A comprehensive evaluation of MODIS-derived GPP for forest ecosystems using the site-based FLUXNET database. *Environmental Earth Sciences* **74**: 5907–5918.

Thomas, R.B., I.C. Prentice, H. Graven, P. Ciais, J.B. Fisher, M. Huang, D.N. Huntzinger, A. Ito, A. Jacobson, A. Jain, J. Mao, A. Michalak, S. Peng, B. Poulter, D.M. Ricciuto, X. Shi, C. Schwalm, H. Tian and N. Zeng (2016) Increased light-use efficiency in northern terrestrial ecosystems indicated by $CO_2$ and greening observations. *Geophysical Research Letters* **43**: 11339–11349.

Togashi, H.F., I.C. Prentice, O.K. Atkin, C. Macfarlane, S.M. Prober, K.J. Bloomfield and B.J. Evans (2018) Acclimation of leaf photosynthetic traits to temperature in an evergreen woodland, consistent with the coordination hypothesis. *Biogeosciences* **15**: 3461–3474.

Ukkola, A.M., I.C. Prentice, T.F. Keenan, A.I.J.M. van Dijk, N.R. Viney, R.B. Myneni and J. Bi (2015) Reduced streamflow in water-stressed climates consistent with $CO_2$ effects on vegetation. *Nature Climate Change* **6**: 75–78.

Verma, M., M.A. Friedl, A.D. Richardson, G. Kiely, A. Cescatti, B.E. Law, G. Wohlfahrt, B. Gielen, O. Roupsard, E.J. Moors, P. Toscano, F.P. Vaccari, D. Gianelle, G. Bohrer, A. Varlagin, N. Buchmann, E. van Gorsel, L. Montagnani and P. Propastin (2014) Remote sensing of annual terrestrial gross primary productivity from MODIS: an assessment using the FLUXNET La Thuile data set. *Biogeosciences* **11**: 2185–2200.

Veroustraete, F. (1994) On the use of a simple deciduous forest model for the interpretation of climate change effects at the level of carbon dynamics. *Ecological Modelling* **75**/**76**: 221–237.

Veroustraete, F., H. Sabbe and H. Eerens (2002) Estimation of carbon mass fluxes over Europe using the C-Fix model and Euroflux data. *Remote Sensing of Environment* **83**: 377–400.

Vicca, S., S. Luyssaert, J. Peñuelas, M. Campioli, F.S. Chapin III, P. Ciais, A. Heinemeyer, P. Högberg, W.L. Kutsch, B.E. Law, Y. Malhi, D. Papale, S.L. Piao, M. Reichstein, E.D. Schulze and I.A. Janssens (2012) Fertile forests produce biomass more efficiently. *Ecology Letters* **15**: 520–526.

von Caemmerer, S. (2000) *Biochemical models of leaf photosynthesis*. CSIRO Publishing, Collingwood, 165 pp.

Wang, H., I.C Prentice, W.M. Cornwell, T.F. Keenan, T.W. Davis, I.J. Wright, B.J. Evans and C. Peng (2017a) Towards a universal model for carbon dioxide uptake by plants. *Nature Plants* **3**: 734–741.

Wang, H., I.C. Prentice, T.W. Davis, T.F. Keenan, I.J. Wright and C. Peng (2017b) Photosynthetic responses to altitude: an explanation based on optimality principles. *New Phytologist* **213**: 976–982.

Wenzel, S., P.M. Cox, V. Eyring and P. Friedlingstein (2014) Emergent constraints on climate-carbon cycle feedbacks in the CMIP5 Earth system models. *Journal of Geophysical Research* **119**: 794–807.

Wenzel, S., P.M. Cox, V. Eyring and P. Friedlingstein (2016) Projected land photosynthesis constrained by changes in the seasonal cycle of atmospheric $CO_2$. *Nature* **539**: 499–501.

Wright, I.J., P.B. Reich and M. Westoby (2003) Least-cost input mixtures of water and nitrogen for photosynthesis. *The American Naturalist* **161**: 98–111.

Yebra, M., A.I.J.M. van Dijk, R. Leuning and J.P. Guerschman (2015) Global vegetation gross primary production estimation using satellite-derived light-use efficiency and canopy conductance. *Remote Sensing of Environment* **163**: 206–216.

Yuan, W., W. Cai, J. Xia, J. Chen, S. Liu, W. Dong, L. Merbold, B. Law, A. Arain, J. Beringer, C. Bernhofer, A. Black, P.D. Blanken, A. Cescatti, Y. Chen, D. Gianelle, I.A. Janssens, M. Jung, T. Kato, G. Kiely, D. Liu, B. Marcolla, L. Montagnani, A. Raschi, O. Roupsard, A. Varlagin and G. Wohlfahrt (2007) Deriving a light use efficiency model from eddy covariance flux data for predicting daily gross primary production across biomes. *Agricultural and Forest Meteorology* **143**: 189–207.

Yuan, Y., S. Liu, G. Yu, J.-M. Bonnefond, J. Chen K. Davis, A.R. Desai, A.H. Goldstein, D. Gianelle, F. Rossi, A.E. Suyker and S.B. Verma (2010) Global estimates of evapotranspiration and gross primary production based on MODIS and global meteorology data. *Remote Sensing of Environment* **114**: 1416–1431.

Yuan, W.,W. Cai, J. Xia, J. Chen, S. Liu, W. Dong, L. Merbold, B. Law, A. Arain, J. Beringer, C. Bernhofer, A. Black, P.D. Blanken, A. Cescatti, Y. Chen, L. François, D. Gianelle, I.A. Janssens, M. Jung, T. Kato, G. Kiely, D. Liu, B. Marcolla, L. Montagnani, A. Raschi, O. Roupsard, A. Varlagin and G. Wohlfahrt (2014) Global comparison of light use efficiency models for simulating terrestrial vegetation gross primary production based on the LaThuile database. *Agricultural and Forest Meteorology* **192**: 108–120.

Zhao, M., F.A. Heinsch, R.R. Nemani and S.W. Running (2005) Improvements of the MODIS terrestrial gross and net primary production data set. *Remote Sensing of Environment* **95**: 164–176.

Zhao, M. and S.W. Running (2010) Drought-induced reduction in global terrestrial net primary production from 2000 through 2009. *Science* **329**: 940–943.

Zhou, S., R. Duursma, B.E. Medlyn, J.W.G. Kelley and I.C. Prentice (2013) How should we model plant responses to drought? An analysis of stomatal and non-stomatal responses to water stress. *Agricultural and Forest Meteorology* **182–183**, 204–214.

Zhu, X.-G., S.P. Long and D.R. Ort (2010) Improving photosynthetic efficiency for greater yield. *Annual Review of Plant Biology* **61**: 235-261.

Zhu, Z. S. Piao, R.B. Myneni, M. Huang, Z. Zeng, J.G. Canadell, P. Ciais, S. Sitch, P. Friedlingstein, A. Arneth, C. Cao, L. Cheng, E. Kato, C. Koven, Y. Li, X. Lian, Y. Liu, R. Liu, J. Mao, Y. Pan, S. Peng, J. Peñuelas, B. Poulter, T.A.M. Pugh, B.D. Stocker, N. Viovy, X. Wang, Y. Wang, Z. Xiao, H. Yang, S. Zaehle and N. Zeng (2016) Greening of the Earth and its drivers. *Nature Climate Change* **6**: 791–795.

Zuur, A.F., E.N. Ieno, N.J. Walker, A.A. Saveliev and G.M. Smith (2009) *Mixed effects models and extensions in ecology with R*. Springer Science, New York.